Lemon Juice-Infused PVA Nanofibers for the Development of Sustainable Antioxidant and Antibacterial Electrospun Hydrogel Biomaterials

*Anna Zakrzewska,[a] Alicja Kosik-Kozioł,[a] Seyed Shahrooz Zargarian,[a] Michele Zanoni,[b] Chiara Gualandi,[b,c,d] Massimiliano Lanzi,[e] and Filippo Pierini[a]**

[a] Department of Biosystems and Soft Matter, Institute of Fundamental Technological Research, Polish Academy of Sciences, Pawińskiego 5B, 02-106 Warsaw, Poland

[b] Department of Chemistry "Giacomo Ciamician", University of Bologna, Via Selmi 2, 40126 Bologna, Italy

[c] INSTM UdR of Bologna, University of Bologna, Via Selmi 2, 40126 Bologna, Italy

[d] Interdepartmental Center for Industrial Research on Advanced Applications in Mechanical Engineering and Materials Technology, CIRI-MAM, University of Bologna, Viale Risorgimento 2, 40136 Bologna, Italy

[e] Department of Industrial Chemistry “Toso Montanari”, University of Bologna, Viale del Risorgimento 4, 40136 Bologna, Italy

*Corresponding Author's e-mail address: fpierini@ippt.pan.pl

ABSTRACT: Cross-linking bonds adjacent polymer chains, into a three-dimensional network. Cross-linked poly(vinyl alcohol) (PVA) turns into a hydrogel, insoluble structure exhibiting outstanding sorption properties. As an electrospinnable polymer, PVA enables the creation of nanofibrous hydrogels resembling biological tissues, thus ideal for nature-inspired platforms. PVA properties are easily adjustable through additives and appropriate cross-linking method. Drawing inspiration from environmentally safe approaches, this work developed a new "green" method of low-temperature PVA cross-linking. Nanofibers were electrospun from a precursor solution of PVA dissolved in fresh lemon juice, stabilized by heating at 60 °C for 7 days, and thoroughly characterized. The obtained nanoplatform demonstrated long-term stability and enhanced mechanical properties. Its biocompatibility was confirmed, and its antibacterial and health-promoting effects were attributed to lemon juice – rich in vitamin C, a potent antioxidant with anti-inflammatory properties. The developed system has future potential for use in the biomedical engineering field as a dressing accelerating wound healing.

KEYWORDS: poly(vinyl alcohol), electrospinning, lemon juice, "green" cross-linking, nanofibrous hydrogel.

1. INTRODUCTION

Polymer cross-linking involves the formation of chemical bonds between different polymer chains, resulting in the development of a three-dimensional network.[1] In the non-cross-linked form, individual polymer chains are linear or branched, with no connections between them. The cross-linking process aims to change the physical and chemical features of the material, with the main improvement being its mechanical properties, thermal behavior, and chemical resistance. What is significant, cross-linked polymers become insoluble in water and other solvents.[2]

Hydrophilic polymers, after cross-linking, turn into hydrogels (HGs) with an exceptional ability to absorb and retain water or body fluids.[1,3] They owe this feature to the presence of hydrophilic groups in their chains.[4] These three-dimensional structures are widely used in various fields, including medicine, specifically wound healing dressings preparation,[5,6] drug delivery systems,[7,8] and tissue engineering.[9,10] Hydrogels can consist of up to 99% water,[11] which makes their physical properties similar to natural human tissues such as skin, muscles, and connective tissue.[1] What is additionally essential, hydrogels are semi-permeable, which means they can allow the passage of small molecules, such as drugs, while also acting as a barrier to larger molecules and microorganisms.[12] This makes them suitable to support healing processes while protecting against infections. Their softness and flexibility allow hydrogels to adapt to the shape of the tissues they come into contact with, reducing the risk of damage and providing patient comfort.[13]

One of the polymers used in the HGs production for medical applications is poly(vinyl alcohol) (PVA). It is a hydrophilic synthetic polymer characterized by excellent biocompatibility, non-toxicity, good mechanical strength, and stability in various environmental conditions.[14] PVA is easy to process, which allows it to be formed into various structures, such as films,[15] gels,[16]

microspheres,[17] and nanofibers.[18] In particular, electrospun nanofibrous hydrogels are ideal for designing nature-inspired platforms due to their mimicry of biological tissues.[19]

Electrospinning is a technique that allows the fabrication of continuous polymer fibers in the nanoscale under the influence of an electric field. In this process, a polymer solution placed in a syringe with a metal needle is ejected after applying a high voltage.[20] Due to the potential difference between the needle and the collector, the liquid stream stretches, which causes the deposition of nanofibers on the grounded surface of the collector.[21]

The properties of PVA nanofibers can be modified by combining the polymer with other substances, such as polymers, drugs, or enzymes. Adjusting properties can also be done by choosing the appropriate cross-linking method. Given the diverse applications of PVA-based materials, selecting the proper cross-linking method is essential for optimizing their performance.[22]

There are many widely known methods of PVA cross-linking, which can be divided into chemical and physical.[23] Chemical cross-linking agents react with hydroxyl groups in the polymer, creating permanent cross-links (covalent bonds) between polymer chains.[24] Among the chemical approaches, exposure to glutaraldehyde vapors[25,26] or immersion in its solution,[27,28] the use of boric acid,[29,30] citric acid[31,32] or another polymer[33] as a cross-linking agent are distinguished. In contrast to this approach, physical cross-linking involves using various physical agents that lead to the formation of hydrogen bonds or other intermolecular interactions.[34] In this case, freezing and thawing,[35] UV irradiation,[36] the addition of glycerol,[37] stabilization with methanol,[38] immersion in ethanol followed by heating,[22] and thermal treatment alone (at relatively high temperatures)[22] should be indicated. The latter method is extremely interesting and is one of the so-called "green" methods, which recently have seen a rapid increase in interest because they are extremely friendly to the environment, not requiring the use of any toxic or harmful substances. Indeed, thermal

treatment is an effective and safe approach that does not affect the polymer structure since PVA is stable over a wide temperature range.[39] However, the great variety of applications of PVA-based materials is due to the possibility of polymer chemical modification and combination with other substances that can degrade or lose their properties, such as enzymatic activity, at high temperatures.

Taking inspiration from environmentally friendly "green" methods, *i.e.*, high-temperature treatment and addition of citric acid followed by heating, an innovative method for PVA cross-linking at low temperature was developed. The nanofibrous hydrogel was prepared by electrospinning the PVA precursor solution containing natural lemon juice, acting as a cross-linking agent, and then exposing the mat to a temperature of 60 °C for 7 days. The acidic pH of natural lemon juice catalyzes the cross-linking process, during which an esterification reaction between the hydroxyl groups of the polymer and the carboxyl groups of citric acid occurs.[32] In this process, the protons present in the acidic medium enhance the electrophilic character of the carbonyl carbon in citric acid, promoting nucleophilic attack by the hydroxyl groups of the polymer. This leads to the formation of covalent ester bonds, which are responsible for the establishment of a three-dimensional cross-linked network. The optimized process conditions allowed obtaining a water-insoluble material with improved mechanical properties, with a higher Young's modulus compared to as spun nanofibers and significantly higher elasticity compared to control PVA samples not enriched with fruit components. The biocompatibility of these materials, as well as health-promoting properties resulting from the presence of lemon juice, such as antioxidant effect corresponding with anti-inflammatory properties, were confirmed. These properties are particularly important for the platform's potential use as a dressing supporting wound healing, especially in case of inflammation. Moreover, materials prepared from two

electrospinning solutions – PVA with lemon juice and PVA with water – were compared. The tested nanoplatforms underwent cross-linking using three different approaches, *i.e.,* the newly developed low-temperature method, high-temperature treatment, and exposure to glutaraldehyde vapors, or were left non-cross-linked. It was shown that using lemon juice is an excellent alternative to previously used approaches and opens the way to developing new PVA-based materials with extended application possibilities without any negative effects on the environment.

2. EXPERIMENTAL SECTION

2.1 Materials

PVA (M_w 85 000−124 000 Da, degree of hydrolysis 99+%), ethanol absolute (EtOH), 50 wt.% glutaraldehyde solution, 25 wt.% glutaraldehyde solution (Grade I, specially purified for use as an electron microscopy fixative), 2,2-diphenyl-1-picrylhydrazyl (DPPH), phosphate buffer saline (PBS), L929 murine fibroblasts and hexamethyldisilazane (HMDS), were obtained from Sigma-Aldrich (Poland). Lysogeny broth agar (LB agar) and lysogeny broth (LB) were obtained from A&A Biotechnology. Gram-positive bacteria *Staphylococcus aureus* (*S. aureus*) ATCC 25923 were obtained from Pol-AURA. Dulbecco's modified Eagle's medium (DMEM), fetal bovine serum (FBS), penicillin-streptomycin (PS), and ethylenediaminetetraacetic acid-trypsin (EDTA-trypsin) were purchased from Gibco Invitrogen (USA). PrestoBlue was bought from Thermo-Fisher Scientific (USA). Lemon juice (pH ≈ 2) was obtained from fresh fruit purchased at the local supermarket.

2.2 Methods

Fabrication of PVA nanofibers from aqueous and lemon solutions through electrospinning

PVA precursor solutions were prepared by dissolving PVA (10% w/v) in Milli-Q deionized water (W) or hand-made 100%lemon juice (L) during heating at 80 °C for 2 h on a magnetic stirrer.

Lemon juice was obtained immediately before precursor solution preparation by squeezing the fresh fruit, centrifuging (15000 RPM, 5 min) using PHOENIX Instrument Micro Centrifuge CD-2012, and then two-stage filtration using syringe filters with a 0.45 μm and 0.20 μm polyethersulfone membrane, respectively. Ethanol was added to both PVA solutions in a ratio of 1:9, and solutions (10 mL each) were electrospun onto a drum collector covered with aluminum foil using an NE300 NanoSpinner chamber, Inovenso. In the process, a 23G needle was used, its distance from the collector was 10 cm, the voltage – 14 kV, and the flow rate – 2 mL h^{-1}.

Cross-linking of nanofibers

Each of the obtained nanofibrous mats was divided into four parts, and one was left non-cross-linked (NC) while the remaining portions were cross-linked using three different approaches. The first one was a "green" treatment at a relatively high temperature of 160 °C for 2 h (160C), the second – an innovative low-temperature approach using a temperature of 60 °C for 7 days (60C), and the last one – a chemical cross-linking consisting of exposure to 1.0 M glutaraldehyde vapors for 24 h (GA). Depending on the solvent used for PVA (W or L) and further processing (NC, 160C, 60C, GA), the nanofibrous samples were assigned the following codes:

W/NC; L/NC;

W/160C; L/160C;

W/60C; L/60C;

W/GA; L/GA.

Water solubility tests and gel content determination

Samples weighing 2.5 mg were cut and placed in separate vials. Each vial was then filled with 800 μL of Milli-Q deionized water, closed, and left at room temperature for 24 h. After this time, the samples were removed from the water and allowed to air-dry for further analysis, including

morphology evaluation using a scanning electron microscope (SEM). Supernatants after solubility tests were also analyzed to check the release of lemon components into the aqueous medium after immersion.

To determine the gel content of all nanofibrous systems, samples weighing approximately 10 mg each were placed in vials into which 10 mL of water was poured. The samples were left in the water for 2 h and then stirred for 10 min. After stirring, the water was pipetted off, and a new portion of the solvent was added. This procedure was repeated three times, then the samples were left to air-dry overnight, and finally placed in a vacuum for 1 h to remove any residual moisture. The dried samples were weighed again, and the percentage of gel was calculated.

Morphological characterization

All electrospun samples, both immediately after fabrication and cross-linking, as well as after water solubility tests, were imaged using a scanning electron microscope (JSM-6010PLUS/LV, In TouchScope microscope). To ensure the samples have the conductivity required for this analysis, they were sputtered with a thin layer of gold using the DII-29030SCTR JEOL Smart Coater. All samples were analyzed using the same beam energy of 5 kV, and each image was taken at a magnification of 2500x.

Spectroscopic analysis

Fourier-transform infrared (FT-IR) spectroscopy. FT-IR analysis of all materials was performed in order to identify functional groups and chemical bonds present in the systems, both before and after water solubility tests. For this purpose, Vertex70, Bruker spectrometer and OPUS 8.1 software were used. The samples were scanned with a resolution of 2 cm^{-1} in the wavenumber range of 4000–400 cm^{-1}.

Ultraviolet-Visible (UV-Vis) spectroscopy. UV-Vis spectroscopy was used to analyze solid-state nanofiber samples, pure lemon juice before and after heating, and to detect its presence in the supernatants after water solubility tests of the nanofibrous mats.

To analyze samples in a solid state, the nanofibers were electrospun onto 2.4 cm×2.4 cm coverslips and then adequately cross-linked. PerkinElmer UV-Vis-NIR Lambda 19 spectrometer equipped with a Labsphere RSA-PE-19 Integrating Sphere was used for the analysis, and absorption spectra were recorded in the 200–800 nm wavelength range. The measurements were repeated after 3 months.

The analysis of lemon juice directly squeezed, centrifuged, and filtered, and juice heated at 80 °C for 2 h was performed using a Multiscan GO absorption spectrometer (Thermo Scientific). For this purpose, several samples of each juice with different concentrations (0−15%) were prepared, and the spectra were recorded in the wavelength range of 200–1000 nm using a quartz cuvette.

After nanofiber solubility tests in water, the supernatants were also subjected to spectrophotometric analysis using a Multiscan GO absorption spectrometer (Thermo Scientific) and a quartz cuvette. These measurements aimed to determine whether and in what amounts lemon juice components were released into the aqueous medium.

Stability of the polymer films in water

A study of the stability of the films in water was performed to check the absorption capacity and water solubility of the films formed from the precursor solutions and, therefore, to check whether lemon juice can act as a cross-linker without additional heat treatment. For this purpose, films were prepared by dropping equal volumes of aqueous and lemon juice PVA precursor solutions on a flat surface and then, after drying, detaching them. The films were weighed immediately after

preparation and then at specified time points in the range of 1 min–24 h after water immersion. After 24 h, films were removed from the water, air-dried, and weighed again.

Thermal analysis

Thermogravimetric analysis (TGA). TGA, aiming to investigate the changes in the mass of a material sample as a function of temperature, was performed using a TA Instruments TGA Q500. The measurements were carried out from room temperature to 600 °C using a heating rate of 10 °C min^{-1} in a nitrogen atmosphere.

Differential scanning calorimetry (DSC). DSC was performed using a TA Instruments Q100 DSC apparatus equipped with a Refrigerated Cooling System (RCS90). Samples were subjected to a first heating scan in the temperature range -90–240 °C at a rate of 20 °C min^{-1}, followed by a controlled cooling at 10 °C min^{-1} to -90°C and a second heating scan at 20 °C min^{-1} to 240 °C. Glass transition temperatures (T_g) were determined at the mid-point of the step-change in the DSC trace. Melting temperatures (T_m) were determined at the endothermic melting peak. The melting enthalpy (ΔH_m) was also measured, and the crystallinity content (χ_c) was evaluated by considering the ΔH_m of a 100% crystalline PVA equal to 161 J g^{-1}.[40]

X-ray diffraction (XRD)

Wide-angle X-ray diffraction measurements (XRD) were carried out at room temperature with a PANalytical X'Pert PRO diffractometer equipped with a fast solid state X'Celerator detector. CuKα radiation was used (40 mA, 40 kV). The 2θ range was from 5° to 60° with a step size of 0.033° and time/step of 20 s.

Mechanical properties

All W and L samples, both non-cross-linked and after cross-linking using three different approaches, were subjected to mechanical testing. Tensile strength measurements were performed using CTXTexture Analyzer (Brookfield Ametek). Three samples with dimensions 1 cm×4 cm were cut from each material, then placed in the apparatus holders and stretched until their breaking point. After placing the sample in the analyzer holders, its initial working length was 2 cm. In each test, data were collected at 50 points s^{-1}, the measurement was started with a trigger load of 0.10 N, and the stretching speed was 1 mm s^{-1}.

Using Texture Pro V1.0 Build19 software, force-displacement curves were recorded, based on which stress-strain dependences were later calculated and plotted. Stress is the ratio of force to the initial area of a sample, and strain describes the change in sample length compared to its initial length. For each sample, after averaging the results from three measurements, Young's modulus was determined. Young's modulus is a measure of the stiffness of a material, which can be calculated as a ratio of stress (the force causing deformation) to strain (a measure of the change in shape or size of a material in response to applied stress) in the linear elastic range.[41]

Photothermal response

Due to the color change of some nanofibrous samples from white to brown due to cross-linking, their photothermal response ability was checked. Towards this aim, NIR laser radiation (MDL-H-808/5W, Changchun New Industries Optoelectronics Tech. Co., Ltd.) with a wavelength of 808 nm and a power of 2500 mW was used. The tests involved nanofiber mats prepared by electrospinning the same volume of PVA solutions (W and L), from which samples of the same size were cut out and further processed or left non-cross-linked. All systems (W/NC, W/160C, W/60C, W/GA, L/NC, L/160C, L/60C, and L/GA) were irradiated until the maximum temperature

was reached and stabilized. After 3 minutes, the laser was turned off, and temperature changes during the entire experiment were observed using a thermal imaging camera (FLIR A655sc, EC TEST Systems) and FLIR Research Studio software. For the sample that showed the best photothermal response, an additional test was performed in both dry and wet conditions, starting from an initial temperature of 37 °C.

In vitro cell study

Cell culture and seeding. Murine fibroblast L929 cells were cultured in DMEM enriched with 10% (v/v) FBS and 1% (v/v) PS. The culture medium was changed every 48 h, and the cells were kept in an incubator set to 37 °C with a 5% CO_2 environment until they covered 80% of the surface area. Upon reaching this confluence, the cells were detached using 0.05% EDTA-trypsin solution, spun down at 1200 RPM for 5 minutes, and quantified. The cell concentration was then adjusted by diluting them in a fresh culture medium to ensure that each sample was seeded with 10 000 cells.[42] In a 24-well plate setup, three types of fibrous samples, L/160C, L/60C, and L/GA, each measuring 1.5 cm in diameter, underwent sterilization via UV irradiation for 30 minutes on each side. After sterilization, these samples were seeded with L929 fibroblasts by carefully placing 50 µL of cell-containing media, with a cell density of 10 000 cells, onto the surface of each sample.[37] Subsequently, 1 mL of DMEM media, supplemented as required, was added to each well. A control group consisting of L929 fibroblasts seeded directly onto glass slides, without the use of fibrous samples, was also prepared and is henceforth referred to as the CTRL group. For all groups, the culture medium was refreshed every 48 h, and the entire culture was sustained for a duration of 7 days.

Cell viability. The PrestoBlue assay was employed to evaluate the viability of cells quantitatively. The fibrous samples and the tissue culture plate seeded with L929 fibroblasts were

subjected to a treatment involving a 10% (v/v) PrestoBlue reagent solution diluted in culture medium. After this treatment, the samples were incubated for 2 h at 37 °C in an atmosphere containing 5% CO_2. Five replicates were prepared and evaluated for each sample type at three distinct time intervals post-cell seeding: 1 day, 3 days, and 7 days. The fluorescence of these samples was quantified using a fluorometer plate reader (Fluoroskan Ascent TM Microplate Fluorometer, Thermo Scientific), with the excitation wavelength set to 530 nm and the emission wavelength set to 620 nm.

Cell morphology. The morphological characteristics of L929 fibroblasts seeded on L/160C, L/60C, L/GA, and CTRL samples were investigated using SEM. This analysis aimed to observe the alterations in cell shape throughout the incubation period. SEM imaging was conducted on three replicates of each sample at specific time points: day 3 and day 7 of the cell culture process. Prior to SEM imaging, the samples underwent a series of preparatory steps. They were first stabilized by being fixed in a 3% solution of ice-cold glutaraldehyde for a duration of 3 h. Following fixation, the samples were rinsed three times with deionized water. To dehydrate the samples, they were sequentially immersed in ethanol solutions of increasing concentration (50%, 70%, 90%, and 100%), with each immersion lasting for 15 minutes. After dehydration, the samples were treated with HMDS and then left to air-dry overnight under a fume hood. The final step involved coating the samples with a thin layer of gold through a sputter-coating process, after which they were ready for examination under the SEM.

Statistical analysis. The data were subjected to statistical analysis using a one-way ANOVA test, followed by Tukey's multiple pairwise comparisons test. These analyses were performed with the aid of Origin 2021 software. The results are presented as the (mean)±(standard deviation) of triplicate measurements, with each mean derived from a set of n=5 samples per group at each

respective time point. The statistical outcomes highlight differences in cell viability among the various groups at each time point. The threshold for statistical significance was set at *p≤ 0.1, **p ≤ 0.01, ***p ≤ 0.001,****p ≤ 0.0001.

Biological activity

Antioxidant properties. Lemon juice, both immediately after preparation and after heating for 2 h at 80 °C, was tested using the DPPH method, commonly used to assess the antioxidant capacity of chemical compounds. DPPH is a stable nitrogen radical that has a characteristic purple color and absorbs light at a wavelength of approximately 517 nm. In the presence of antioxidants, DPPH is reduced, which leads to discoloration of the solution and, thus, a decrease in absorbance.[43] Test samples were prepared by adding 0.1 mM ethanolic solution of DPPH to water and/or lemon juice to obtain final solutions with a DPPH/water/lemon juice ratio of 50/50/0, 50/20/30, 50/40/10, and 50/49/1. Then, the samples were incubated at 37 °C for 2 h and subjected to spectrophotometric analysis using a Multiscan GO absorption spectrometer (Thermo Scientific). The absorbance maximum determined for an aqueous DPPH solution was 522 nm; therefore, the measurements focused on this wavelength. The obtained results were used to calculate lemon juice's free radical inhibition capacity at different concentrations. The following formula was used:

$$\%inhibition = \left(\frac{A_0 - A_t}{A_0}\right) \times 100$$

where A_0 is the absorbance of DPPH solution without antioxidant, and A_t is the absorbance of DPPH solution with antioxidant after incubation at 37 °C for 2 h.

Bacteria culture. The strain *Staphylococcus aureus*, specifically the ATCC 25923, was cultured on LB agar and then isolated through the streak plate method. A single colony was inoculated into fresh LB broth (3 mL) and incubated at 36 °C overnight in an orbital shaker set at 180 RPM in preparation for subsequent experiments.

Qualitative antibacterial activity studies. Circular samples of W/60C and L/60C, each measuring 9 mm in diameter, were sterilized under UV light for 1 h on both sides. An overnight culture of *S. aureus* bacteria was diluted in sterile PBS to 10^6 colony-forming units (CFU) mL^{-1}. A transferring loop was used to evenly disperse 100 µL of the resulting diluted bacteria suspensions on the surface of the agar medium slope. Next, the samples were placed on them. The control sample (CTRL) consisted of plates solely inoculated with bacteria. The samples were incubated overnight at 36 °C for macroscopic visualization.

Quantitative antibacterial activity evaluation. Circular samples of W/60C and L/60C, each measuring 6 mm in diameter, were sterilized under UV light for 1 h on each side and then attached to the bottom of the 96-well plates. A dilution of the *S. aureus* colony, containing 10^6 CFU mL^{-1}, was added to each sample in a volume of 100 µL. A pure bacterial suspension was used as a positive control. The samples were then incubated for 3 h at 37 °C. After incubation, the solutions were moved to a new 96-well plate and serially diluted before plating on LB agar plates. The number of bacterial colonies was counted following an overnight incubation at 36 °C to evaluate bacterial survival.[37]

3. RESULTS AND DISCUSSION

The fabrication process of PVA nanofibers by electrospinning, both from aqueous and lemon juice solutions, is shown schematically in Figure 1a. As a result of heating, the lemon juice changes its color suggesting chemical modifications occurring in its composition. Figure 1b presents the cross-linking of nanofibers by three different methods, *i.e.*, heating at 160 °C for 2 h (160C), heating at 60 °C for 7 days (60C), and exposure to 1.0 M glutaraldehyde (GA) vapors. The optimal conditions for low-temperature cross-linking were determined experimentally (Figure S1). The

resulting nanoplatforms represent nanofibrous hydrogels that have been extensively characterized to highlight differences in the effects of cross-linking methods and their impact on the properties and potential applications of nanofibrous systems.

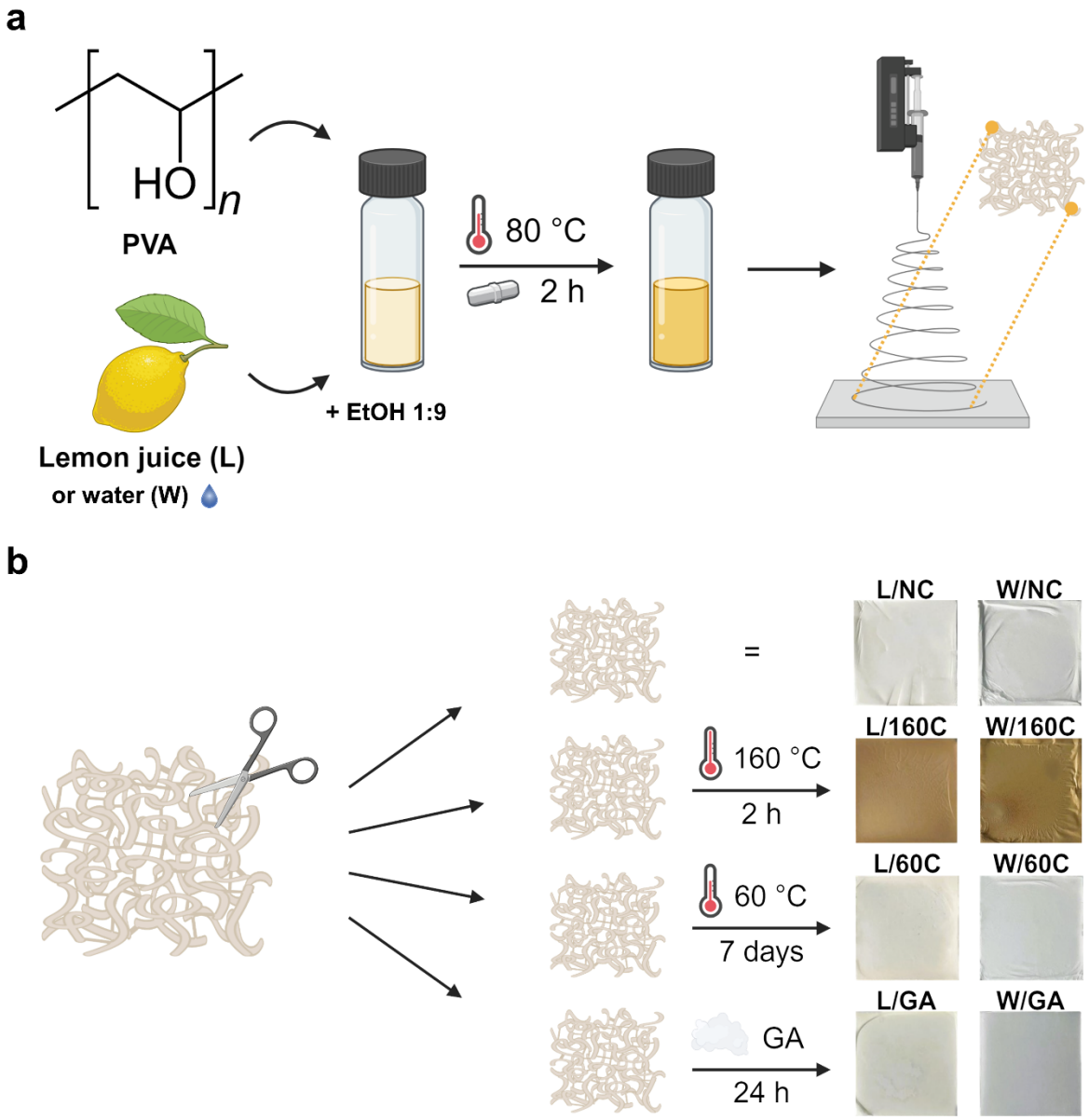

Figure 1. Graphical representation of the fabrication process of PVA-based nanofibrous hydrogels. a) Scheme of the preparation of precursor solutions for electrospinning. b) Scheme of the applied cross-linking approaches. Each of the electrospun mats was divided into four parts,

one of which remained non-cross-linked, two were subjected to thermal treatment (2 h at 160 °C and 7 days at 60 °C), and the last one was exposed to glutaraldehyde vapors (1.0 M, 24 h).

3.1 Water solubility tests and morphological characterization

Water solubility testing of samples is the primary test that was performed to confirm the cross-linking of the nanofibers. Highly cross-linked PVA formulates an insoluble matrix, so visual observation of the material after immersion in water allows preliminary considerations about the effectiveness of the selected cross-linking approach. A schematic representation of the performed test is shown in Figure S2a. In this experiment, residual material was observed in each of the 8 vials after 24 h of water immersion. In the case of the 160C and GA methods, these were quite stiff nanofiber samples that retained their shape. Samples after cross-linking using the 60C method were much softer and more flexible, and the non-cross-linked samples resembled transparent films that were difficult to handle because they curled and were easily damaged, however, the samples containing lemon juice were slightly more resistant.

Visual observation was supported by SEM analysis. Non-cross-linked and three-way cross-linked samples, both immediately after fabrication and after solubility testing, were imaged using SEM (Figure 2). This analysis proved that nanofibers electrospun from W and L solutions are continuous, have cylindrical shape and random orientation. The surface of all nanofibers is smooth, without beads, although differences in the diameter of individual nanofibers can be noticed in the case of material electrospun from an aqueous solution. Additionally, each of the three cross-linking approaches used did not affect the morphology of the nanofibers, including their cylindricity, smoothness, and diameter. This is an interesting observation because the insets in the SEM images, which represent macroscopic photos of fabricated materials, show their color change under the

influence of temperature. This indicates the thermal degradation of the samples and a change in their specific properties.

Imaging of samples after water solubility tests revealed further important facts. The W/NC sample has completely lost fibrous morphology, and its surface became smooth, while the L/NC sample retained porosity. Nevertheless, the film-like structure is observed in both materials. The W/160C and L/160C nanofibers were preserved intact, as was L/GA. Although the morphology of the L/60C sample changed after water immersion, fiber remain visible in SEM images. In the case of W/60C, only a slight residue of nanofibers is visible, and in W/GA, a significant change in the morphology of the nanofibers is observed since some of them fused, creating locally thicker structures. The gel content of the samples was determined as 1) 35.9% and 37.5% for W/NC and L/NC; 2) 97.5% and 98.8% for W/160C and L/160C; 3) 65.5% and 71.2% for W/60C and L/60C; 4) 89.4% and 61.5% for W/GA and L/GA, respectively (Table S1).

The obtained results suggest that the presence of lemon extracts in the fibers favors the cross-linking of PVA and its stability against water dissolution when compared with samples electrospun from aqueous solution and subjected to the same cross-linking procedures. This indicates the potential of the developed "green" method for achieving eco-friendly PVA-based nanostructured hydrogels provided with additional features resulting from the health properties of natural lemon juice.

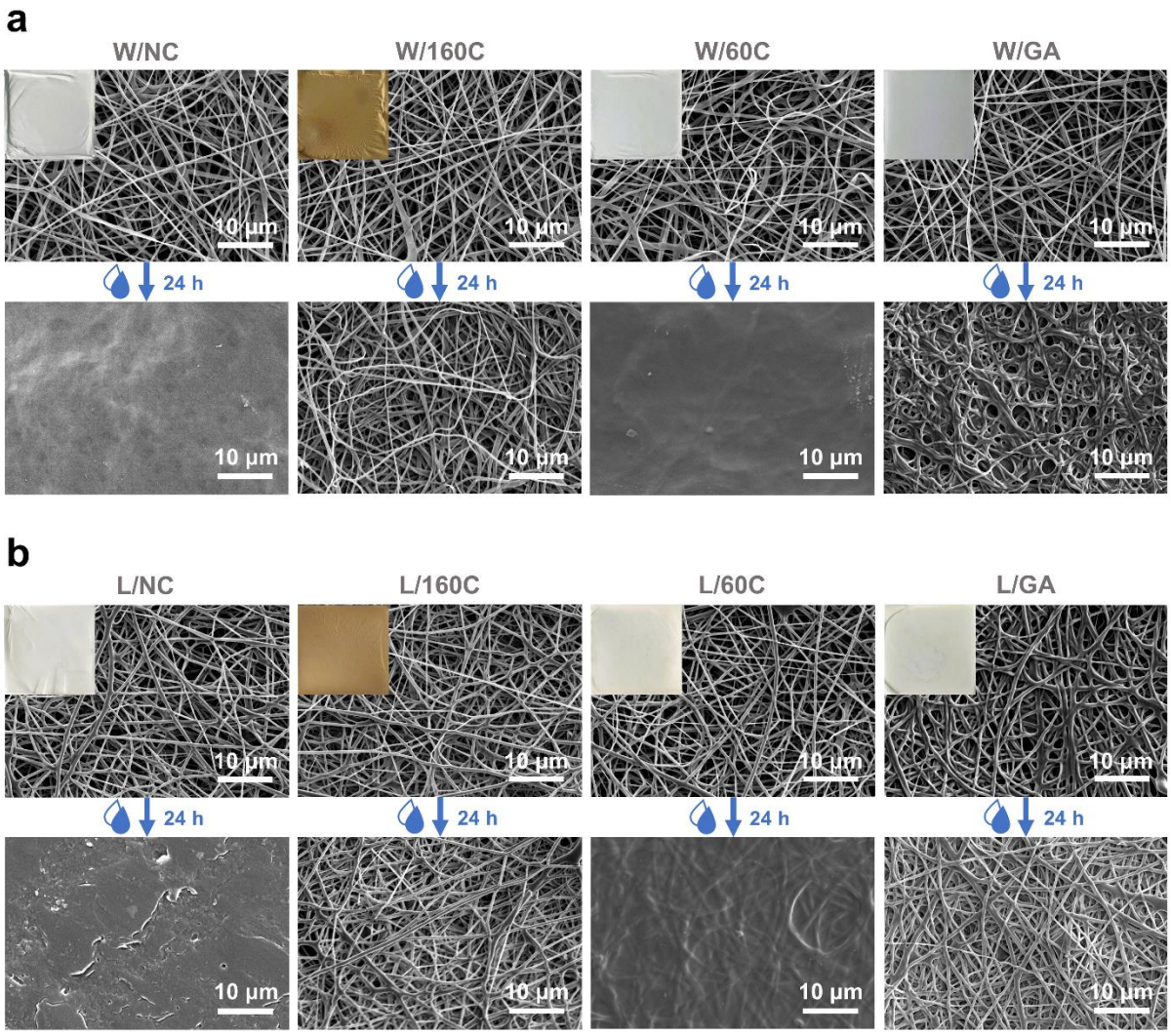

Figure 2. Morphological characterization of nanofibers and evaluation of cross-linking methods efficiency based on water solubility tests. a) SEM images of nanofibers electrospun from aqueous solutions (non-cross-linked and cross-linked using three selected methods), both before and after immersion in water for 24 h. b) SEM images of nanofibers electrospun from lemon juice solutions (non-cross-linked and cross-linked using three selected methods), both before and after immersion in water for 24 h. The insets show camera photos of individual samples with actual dimensions of 2.4 cm×2.4 cm.

3.2 Spectroscopic analysis

Fourier-transform infrared (FT-IR) spectroscopy. The FT-IR spectra of W/NC, W/160C, W/60C, and W/GA nanofibers, before and after the solubility tests, are shown in Figure 3a. The peak with the maximum at 3276 cm^{-1} is due to the stretching vibrations of hydroxyl groups (–OH). An extensive hydrogen bond network explains the large peak width in the spectrum. Two subsequent peaks at 2940 and 2904 cm^{-1} are related to the asymmetric and symmetric stretching vibrations of methylene groups ($–CH_2$). The peak at the wavenumber of 1408 cm^{-1} refers to the deformation vibrations of $–CH_2$ groups, while the one at 1315 cm^{-1} is the result of the $–CH_2$ and −OH bending. The small peak at 1257 cm^{-1} in the spectra is due to the stretching vibrations of the –C–O– bond at the −OH groups, while the peaks at 1140 and 1084 cm^{-1} are related to the stretching vibrations of the acetal linkage (–C–O–C–), characteristic of ether bonds.[44,45] The peak at 1140 cm^{-1} appears only after cross-linking of the nanofibers by any of the three analyzed methods, confirming the successful completion of this process in each case. The relative intensity of this vibration band is correlated with the crystallinity of the PVA samples,[46] and the highest value can be noted for nanoplatform cross-linked by the 160C method. As expected, all the cross-linked materials are more crystalline than the non-cross-linked ones due to polymer annealing at temperatures promoting the formation of intramolecular hydrogen bonds during the cross-linking process. Additionally, cross-linking of the nanofibers causes a decrease in the absorbance intensity at 3276 cm^{-1} as formed bonds reduce the number of free hydroxyl groups. However, after the solubility tests, the overall intensity and positions of other peaks changed slightly, indicating a possible rearrangement of the PVA network structure or partial dissolution of the insoluble fraction.

Replacing water with lemon juice at the stage of nanofiber fabrication induces some changes in their FT-IR spectra, which reflect chemical interactions between PVA and lemon juice components. In Figure 3b, a broadening of the peak at 3264 cm^{-1} can be observed, resulting from the incorporation of additional hydroxyl groups from citric acid into the system and the formation of hydrogen bonds with PVA groups. In the spectra of L/NC, L/160C, L/60C, and L/GA, there is also a new peak at 1720 cm^{-1}, which is characteristic of the stretching of carboxyl groups (composed of carbonyl units –C=O and hydroxyl units –OH) present in citric acid.[47,48] The presence of additional hydroxyl groups from citric acid also increases the abundance of –C–O– stretching vibrations in the whole system, which results in a significant increase in the intensity of the peak at 1257 cm^{-1}. Moreover, the cross-linking process itself is more visible in the case of samples L than W, which is evidenced by a more significant decrease in the intensity of the peak at 3264 cm^{-1} and its flattening, indicating a greater decrease in the number of free hydroxyl groups. However, analysis of the peak at 1138 cm^{-1} proves that lemon juice components reduce the degree of crystallinity of PVA-based nanostructured systems by disrupting the regular crystal structure of the polymer. Among the samples subjected to cross-linking processes, L/160C is characterized by the lowest degree of crystallinity.

Ultraviolet-Visible (UV-Vis) spectroscopy. The UV-Vis spectra of the solid-state nanofibrous samples are shown in Figure 3c (top – samples W and bottom – samples L). It can be seen from the spectra of samples W/NC, W/160C, W/60C, and W/GA that the pure, non-cross-linked PVA fibers show only a small absorption with a peak maximum at 280 and 330 nm. This is related to the $\pi \rightarrow \pi^*$ and $n \rightarrow \pi^*$ transitions due to the resonating carbonyl group.[49] However, in the visible range, absorption peak is not observed as PVA has a simple chemical structure that lacks functional groups (chromophores) capable of absorbing light with a longer wavelength. Cross-linked PVA

shows increased absorption in the UV-Vis range because the cross-linking process introduces new functional groups to the system (including the already present in the system carbonyl group) and increases electronic conjugation – π electrons are delocalized over a long part of the polymer chain, which reduces the energy required for electronic transition and shifts absorption to longer wavelengths.[50,51]

The addition of lemon juice to PVA significantly affects its UV-Vis spectrum. The L/NC sample shows stronger absorption compared to W/NC, which can be explained by the presence of citric acid, rich in –C=O functional groups absorbing light in the UV range[52] (<380 nm)[53]. Moreover, flavonoids and other polyphenolic compounds present in lemon juice can absorb light in both the UV and Vis range (380>750 nm).[53,54] It should also be noted that citric acid can react with hydroxyl groups in PVA, leading to changes in the chemical structure of the polymer. Therefore, a shift in the position of typical PVA-related peaks and their intensity is observed in the spectra.

Reanalysis of the same samples after 3 months (insets in Figure 3c) provides important information on the stability of the systems. In both W and L samples, the best stability is achieved by the temperature-cross-linked materials. Moreover, the stability is higher for the samples containing lemon juice than for the water-based ones. The loss of stability may be related to the aging of the material and its degradation, *e.g.*, under the influence of contact with oxygen from the air. In the case of lemon juice, which contains ascorbic acid with antioxidant properties, it can be assumed that it neutralizes free radicals responsible for the oxidation of the material.

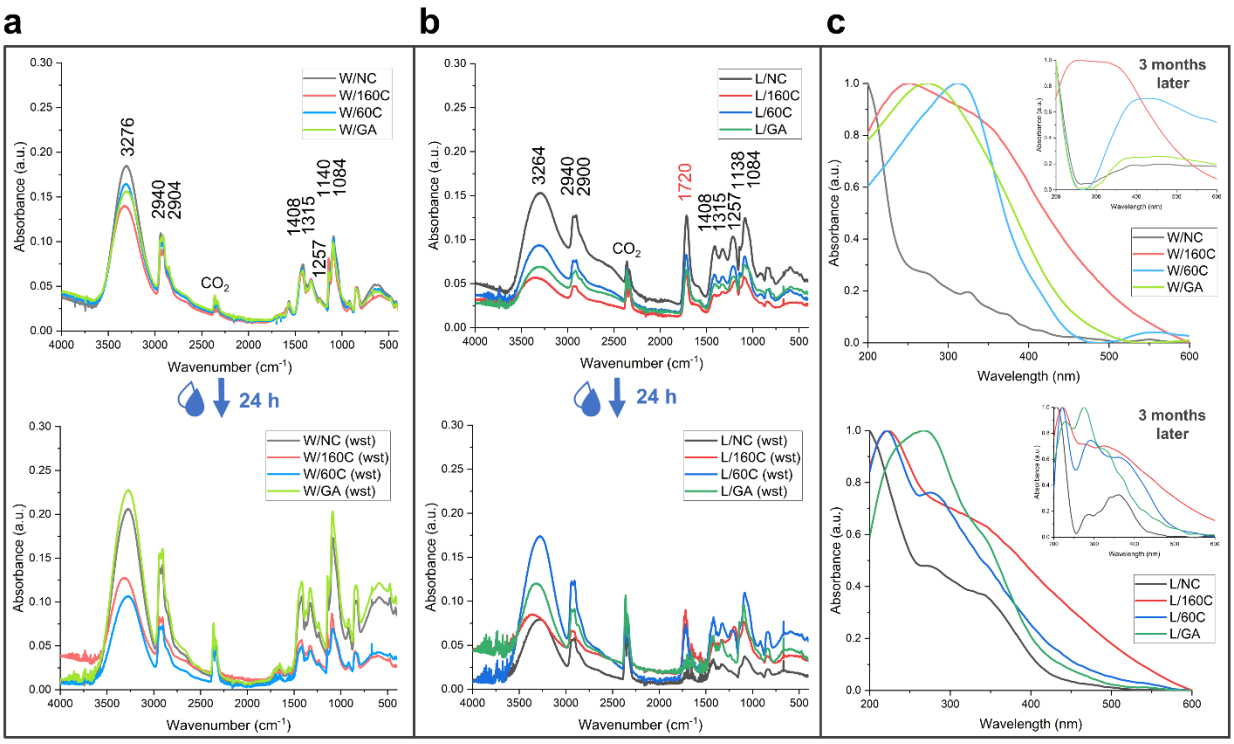

Figure 3. Physico-chemical characteristics. a) FT-IR spectra of nanofibers electrospun from aqueous solution (W/NC, W/160C, W/60C, and W/GA) before and after water solubility tests. b) FT-IR spectra of nanofibers electrospun from lemon juice solution (L/NC, L/160C, L/60C, and L/GA) before and after water solubility tests. c) UV-Vis spectra of solid-state samples (top – samples W and bottom – samples L). Insets show spectra recorded a second time for the same samples after 3 months.

Pure lemon juice was also subjected to spectrophotometric analysis, both immediately after preparation and after heating at 80 °C for 2 h. The latter measurement was important because the preparation of precursor solutions for electrospinning involves such a heating step to dissolve PVA in the solvent used. Visual observation of the juice before and after heating indicates some transitions as the lemon juice changes its color from slightly yellowish to yellow, as shown in Figure 4a. Figure 4b presents the spectra of lemon juice aqueous solutions, varying in concentration, before heating. The absorbance maximum in this case is 335 nm, while the heated

juice shows an absorbance maximum of 282 nm, as shown in Figure 4c. The observed shift to shorter wavelengths may be caused by many factors related to chemical and physical changes occurring during heating. Flavonoids and other polyphenolic compounds can undergo thermal degradation. The decomposition of these compounds leads to the formation of products with a simpler structure, in which electrons are less delocalized, which causes a blue shift in absorption. Another compound present in lemon juice that can undergo thermal degradation is ascorbic acid. Moreover, many components of lemon juice are difficult to identify,[55] and it should be noted that heating can initiate chemical reactions between them, leading to the formation of new compounds that absorb light at other wavelengths.

Figures 4d, e show the UV-Vis spectra of the supernatants after the water solubility tests of samples W and L, respectively. The supernatants in which pure PVA was tested (samples W) do not show strong UV-Vis absorption peaks because this polymer does not contain chromophores absorbing light in the tested range. Small peaks in the UV range may indicate that PVA has partially decomposed. A different situation is observed for the supernatants after the solubility tests of L samples. In each analyzed case, it can be seen that lemon juice was released into the aqueous medium, but the absorbance maximum is slightly shifted concerning 282 nm. There are many potential reasons for this result. PVA can form complexes with organic acids, flavonoids, or other lemon juice components, leading to changes in the UV-Vis spectrum. It is also possible that not all ingredients of lemon juice may be equally soluble in the presence of PVA. Selective solubility may lead to a change in the absorption profile as some components may be present at lower concentrations or be completely absent in the supernatants. The calibration curve and quantitative results are shown in Figure S2b, c.

3.3 Stability of the polymer films in water

The next step was to check how the PVA films would behave after immersion in water. A series of measurements were carried out, in which the W and L films were weighed both in a dry state and at different time intervals after water immersion (1 min–24 h). The results are presented in Figure 4f. From the obtained results, it can be concluded that films W have a greater water absorption capacity than films L, and after water immersion, they can achieve a 5-fold increase in their initial mass. For the samples with lemon juice, this increase is about 3-fold, and in both cases, this state is achieved after 30 minutes. However, the films partially dissolved in water, as they were not subjected to any cross-linking processes. After 24 h in water and then drying, the W and L films were 77.15±2.33% and 48.05±4.60% of their initial mass, respectively.

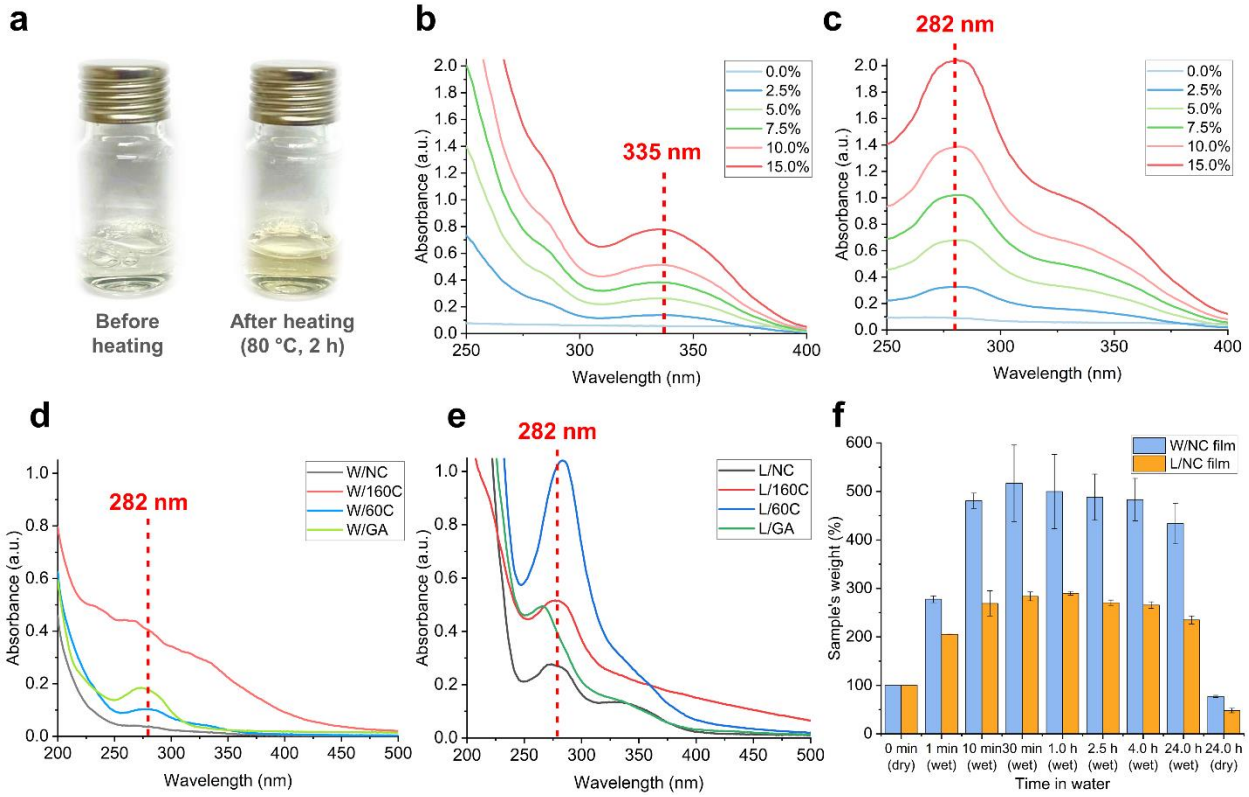

Figure 4. Spectrophotometric analysis of lemon juice and evaluation of the materials' behavior in water. a) Camera photos of vials containing lemon juice before and after heating (a necessary step

in the precursor solution preparation leading to PVA dissolution). b) UV-Vis spectra of unheated lemon juice varying in concentration. The absorption maximum occurs at a wavelength of 335 nm. c) UV-Vis spectra of lemon juice heated at 80 °C for 2 h and varying in concentration. The absorption maximum occurs at a wavelength of 282 nm. d) UV-Vis spectra of the supernatants after the water solubility tests of samples W. e) UV-Vis spectra of the supernatants after the water solubility tests of samples L. f) Behavior of PVA films in water.

3.4 Thermal analysis

Thermogravimetric analysis (TGA). TGA analysis was performed to investigate the thermal stability of the developed nanofibrous hydrogels and to understand how the individual components of the systems decompose with heating. Figure 5a, b shows the mass changes of all samples (top – samples W, bottom – samples L) as a function of temperature and its first derivative. Figure S3 shows a comparison of individual samples, non-cross-linked and cross-linked by a specific method. In the TGA plots for samples prepared from aqueous solutions (W), a small mass loss is observed in the temperature range of 33–82 °C. This is probably related to the evaporation of water adsorbed on the nanofiber surface. However, in the case of W/160C, this mass loss is noticeably smaller, and it can be assumed that the prior cross-linking at 160 °C already removed water from the sample. The main mass loss, related to depolymerization and decomposition of the polymer chain, occurs in the temperature range 200–320 °C in the case of W/NC, W/60C, and W/GA, while for W/160C, a degradation is observed at higher temperatures (220–360 °C). This shift is because part of the thermal degradation previously occurred at 160 °C. Above 400 °C, the decomposition of residual organic groups takes place, and the TGA curves reach a plateau. TGA curves for samples enriched with lemon juice (L) differ, which results from the presence of organic acids (mainly citric acid), sugars, vitamins, various phenolic compounds, and other organic substances

in these systems. Apart from the initial evaporation of water at <80 °C, another mass loss is observed in the range of 100–230 °C for L/NC, L/60C, and L/GA. This loss is related to the degradation/volatilization of lemon juice components and is about 20% w/w. However, it is not observed for L/160C, where decomposition/volatilization apparently occurred during the cross-linking stage. Following the main decomposition at 230–380 °C, the residual organic groups break down, and the TGA curves become steady.

Differential scanning calorimetry (DSC). DSC analysis allows to determine polymer thermal properties and gain information about solid-state polymer structure. According to the literature, the PVA used in the present work has a T_g of around 70 °C and a T_m of around 220 °C.[56] Based on TGA results, W samples are thermally stable up to 200 °C, while L samples display a significant weight loss starting at 100 °C. For this reason, DSC analysis of W samples is feasible (Figure 5c), albeit minor thermal degradation during DSC analysis cannot be excluded. In contrast, the low thermal stability of L samples prevents the acquisition of meaningful data using this technique (Figure S4).

In the first heating scan (Figure 5c – top), all curves display a broad endothermic peak in the 50–120 °C range due to absorbed water evaporation, which prevents the detection of the glass transition temperatures (T_g). At higher temperatures, the curves show a narrow endothermic peak related to the melting of the PVA crystal phase. Table 1 reports the corresponding melting enthalpies (ΔH_m), melting temperatures (T_m), and the calculated degrees of crystallinity (χ_c). It comes out that after the different cross-linking treatments, all samples are semicrystalline, with different amounts of crystal phase. As a matter of fact, the crystallinity degree and crystal morphology are affected not only by polymer architecture and cross-linking density but also by the thermal history of the sample. Therefore, direct comparisons of DSC first heating scans across

the differently treated materials are not meaningful. More information can be obtained by analyzing the second DSC heating scans performed after erasing sample thermal histories (Figure 5c – bottom and Table 1).

After a controlled cooling at 10 °C min^{-1}, the W/NC sample develops a 38% crystal phase, with a T_g at 72 °C and a T_m at 223 °C. In comparison, both W/60C and W/GA samples display slightly higher T_g values and develop a lower amount of crystal phase that melts at slightly lower temperatures. The W/160C sample shows a significantly higher and broader T_g centered at 90 °C, and its crystallinity degree is only 14%. These calorimetric data suggest that W/60C and W/GA samples are partially cross-linked, while the cross-linking degree in W/160C is high. Indeed, the presence of cross-linking points is expected to raise polymer T_g and hinder its capability to crystallize.

Table 1. DSC calorimetric data of W samples: T_g – glass transition temperature determined at the mid-point of the step-change transition; ΔC_p – specific heat capacity; T_m – melting temperature determined at the minimum of the most prominent endothermic melting peak; ΔH_m – melting enthalpy.

Sample	**T_g [°C]**	**ΔC_p [J g^{-1} °C^{-1}]**	**T_m [°C]**	**ΔH_m [J g^{-1}]**	**χ_c [%]**
1st heating scan					
W/NC	n.d.	n.d.	227	66	41
W/160C	n.d.	n.d.	210	66	41
W/60C	n.d.	n.d.	227	60	37
W/GA	n.d.	n.d.	224	75	47
2nd heating scan after controlled cooling					
Sample	**T_g [°C]**	**ΔC_p [J g^{-1} °C^{-1}]**	**T_m [°C]**	**ΔH_m [J g^{-1}]**	**χ_c [%]**
W/NC	72	0.38	223	61	38
W/160C	90	0.74	190	22	14
W/60C	74	0.41	221	57	35
W/GA	76	0.41	220	57	35

n.d. – not detectable due to the presence of the endothermal enthalpy related to absorbed water evaporation

3.5 X-ray diffraction (XRD)

X-ray diffraction provides important information on the crystal structure and degree of crystallinity of the studied samples. Figure 5d (top) shows the XRD profiles of nanofibers electrospun from aqueous solutions, both before and after cross-linking using three different approaches. Each curve shows a main, sharp peak around $2\theta \approx 19°$, confirming that the sample contains crystalline regions typical for PVA.[57] However, the XRD pattern of W/160C differs, showing a narrower diffraction peak at $2\theta \approx 19°$ compared with the other samples and other peaks typical of the PVA crystal phase at $2\theta \approx 11°$, 16°, and 23°, indicating a higher quality of crystal phase.[58] This is consistent with the thermal annealing carried out at 160 °C, which contributes to improving the perfection of PVA crystals in this specific sample. XRD analysis confirms the presence of crystal phase also in the nanofibers enriched with lemon juice. In Figure 5d (bottom), the main diffraction peak of the PVA crystal phase at $2\theta \approx 19°$ can be observed for all of the L samples. Additional peaks at $2\theta \approx 14°$ and 17° present in L/NC, L/GA, and L/60C may be ascribed to citric acid,[59,60] which is present in lemon juice in large quantities. This compound disappears after high-temperature treatment. Similarly to W/160C, the L/160C sample shows crystals of bigger dimensions, consistent with the thermal annealing.

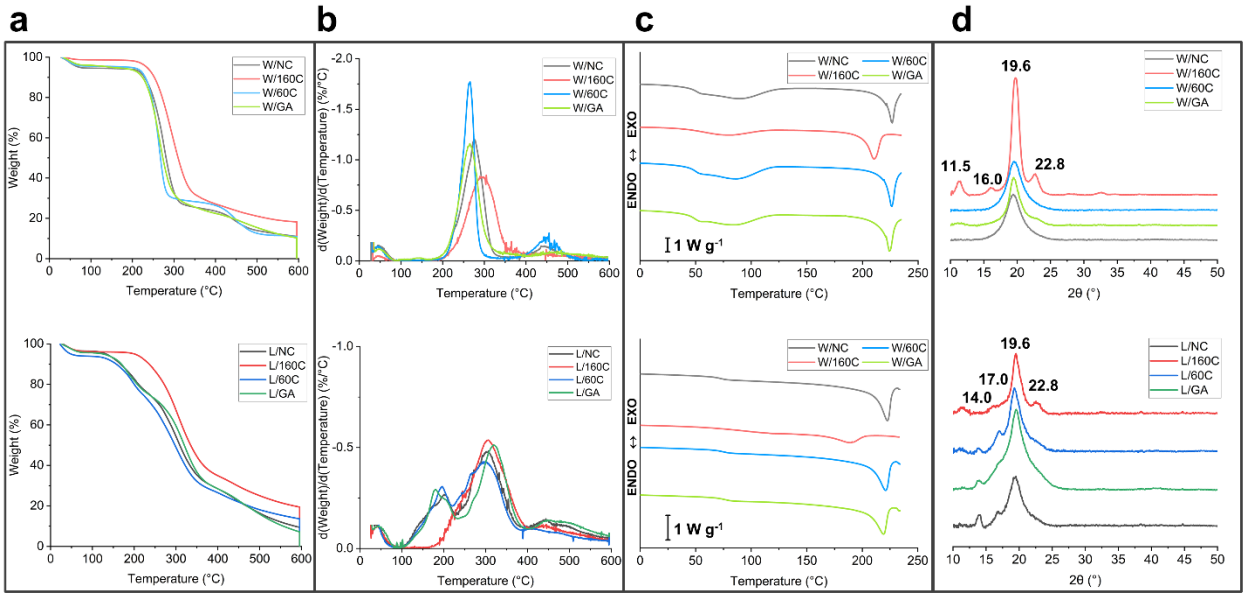

Figure 5. Thermal properties and crystallinity evaluation. a) TGA graphs showing the mass change over time of samples without (W) and with lemon juice (L) and b) the first derivative of this function; (top – samples W, bottom – samples L). c) First DSC heating scans (top) and second DSC heating scans of W samples (bottom). d) XRD diffraction patterns of W samples (top) and L samples (bottom).

3.6 Mechanical properties

In order to compare the mechanical properties of PVA nanofibers prepared from aqueous solutions and those containing lemon juice, as well as to investigate the effect of cross-linking methods on these properties, tensile tests were carried out. The three main steps of this test are shown schematically in Figure S5a. For each material, three repetitions were performed, which consisted of placing the sample in the clamps of the texture analyzer and then stretching (Figure 6a) until it ruptured. Values of Young's modulus are presented in Figure 6b. The first important observation is that the W/NC samples are much stiffer than the L/NC samples, but this situation changes after the cross-linking processes. The highest stiffness is shown by the temperature-cross-linked L samples, so it can be assumed that they are characterized by the highest cross-link density.

As a result of cross-linking, the polymer chains are permanently bonded to each other along their length, creating a three-dimensional network.[61] These connections limit the possibility of free movement of the polymer chains relative to each other, so the material becomes stiff and less susceptible to deformation. This means that at a given stress, the deformation will be smaller compared to the non-cross-linked material.[1] The higher stiffness of the cross-linked L nanofibers compared to the cross-linked W samples (Figure S5b) can be explained by the properties of lemon juice and the interactions between the juice components and the polymer chains, *e.g.*:

1) L samples are stabilized by an esterification reaction that occurs between the hydroxyl groups of the polymer and the carboxyl groups of citric acid, while the main interactions that stabilize the W samples are hydrogen bonds;

2) Citric acid can act as a catalyst in the cross-linking process. Therefore, an acidic environment promotes the formation of stronger or more numerous hydrogen bonds, leading to the formation of a dense and well-ordered network;

3) Flavonoids and other organic acids can form additional hydrogen bonds with the hydroxyl groups of PVA.

The next parameter calculated was the strain of the material achieved immediately before the breaking point, which is shown in Figure 6c. The non-cross-linked nanofibers are naturally characterized by the highest deformability and could be elongated by about 70% and 120%, in the case of W/NC and L/NC, respectively. The deformation capacity of cross-linked materials decreases, which correlates with the increase in their stiffness.[62] However, the samples cross-linked at 160 °C are the least deformable because, in this process, the PVA nanofibers are rapidly dried by evaporation of water, which acts as a plasticizer, and the cross-linking density is higher. Samples cross-linked at lower temperatures, *i.e.*, W/60C and L/60C, turned out to be the most

deformable, so it can be concluded that the proposed method is effective and leads to the formation of an optimal amount of chemical bridges between polymer chains. The amount of formed bonds can strengthen the material structure, but not enough to restrict the mobility of the polymer chains significantly. Furthermore, a temperature of 60 °C corresponds to the glass transition temperature range of PVA (around 50–80 °C),[63,64] meaning that the polymer chains become more mobile and can move more easily relative to each other during cross-linking. The greater mobility of the chains promotes even distribution of the cross-links and maintains the flexibility of the material after cooling.

3.7 Photothermal response

The color change of the nanofibrous samples after the cross-linking processes, especially at high temperature, became the trigger for studying their photothermal properties. The measurement setup is schematically shown in Figure 6d. Figure 6e shows the test results for sample W, the initial temperature of which was 23 °C. PVA is not a polymer capable of photothermal response; therefore, as expected, the temperature of W/NC did not change significantly under the influence of NIR radiation. Similar results were obtained for samples W/60C and W/GA. Interestingly, the sample W/160C quickly reached a temperature of 50 °C as a result of irradiation, which slowly increased to 53 °C over time. Similar behavior was observed for samples L with the same initial temperature (Figure 6f). The temperature of L/NC and L/60C samples did not change significantly; L/GA temperature was elevated by only 6 °C, and for L/160C, a rapid increase in temperature was noted to 53 °C, which then plateaued. However, it should be mentioned that when the initial temperature was 37 °C, which was close to the human body temperature, the W/160C and L/160C materials reached temperatures of 57 °C and 61 °C, respectively (Figure S6). The photoresponsivity of W/160C and L/160C samples to NIR radiation can be explained by the

formation of unsaturated double bonds as a consequence of water elimination[65] during high-temperature cross-linking, resulting in fiber color change and increased absorption of NIR light, which is then converted into heat. Obtained results are promising for the potential application of the developed materials in the field of biomedical engineering, *e.g.*, for the elimination of certain bacteria, in phototherapy or thermal patches.

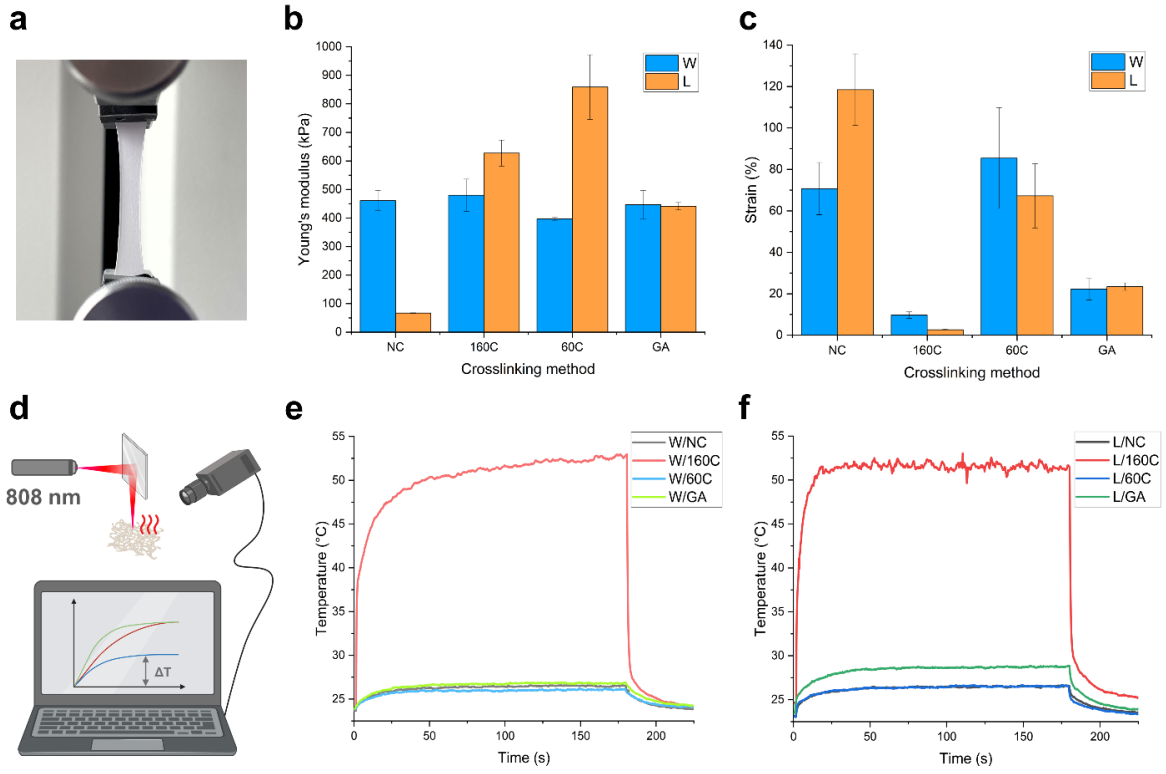

Figure 6. Mechanical properties and photothermal response of the developed nanofibrous systems. a) Camera photo of a nanofibrous sample in the grips of a texture analyzer during tensile tests. b) Graph showing Young's modulus of samples without and with lemon juice, both non-cross-linked and differing in cross-linking methods. c) Strain at break of PVA-based materials. d) Schematic diagram of the experimental setup for testing photothermal properties consisting of NIR laser, thermal camera, and computer. e) Photothermal response of systems prepared from aqueous solutions (W) after NIR irradiation at room temperature. f) Photothermal response of systems containing natural lemon juice (L) after NIR irradiation at room temperature.

3.8 *In vitro* cell study

The *in vitro* biological response was assessed by monitoring the viability of L929 fibroblast cells cultured on L/160C, L/60C, L/GA, and CTRL samples over a 7-day period. Fundamental differences in proliferation are evident among the various groups. In the developed group utilizing "green" cross-linking with a low temperature of 60 °C, there is a 6-fold increase in the absorbance signal after 7 days of incubation compared to day 1. A similar, albeit slightly lower, cell viability with a 5-fold increase in proliferation after 7 days of incubation is observed for the PVA group cross-linked at 160 °C. Essentially, the lowest cell survival was for the PVA group cross-linked with glutaraldehyde vapors, where the cells only increased their proliferation 2.6 times (Figure 7a).

SEM images taken at various time points during cell proliferation showed clear evidence of cell spreading and growth on the sample surfaces, with no significant differences among the conditions tested (Figure 7b, c). During the 3-day period after seeding, the cells appeared round with discernible attachment sites to the samples. As incubation continued, the cells proliferated and entirely covered the surfaces of the fibrous samples, ultimately forming multilayered cell clusters, as vividly shown on day 7 of incubation. Qualitative imaging of cell morphology confirmed the quantitative proliferation studies, where overall, there is a greater number of cells on day 7 of incubation in the following order: L/60C, L/160C, CTRL, and L/GA samples. These results confirm the biocompatibility of the fibrous structures, highlighting their appropriateness for cell attachment, survival, spreading, and proliferation. The cells exhibited normal proliferation in all instances, as indicated by their observed morphology.

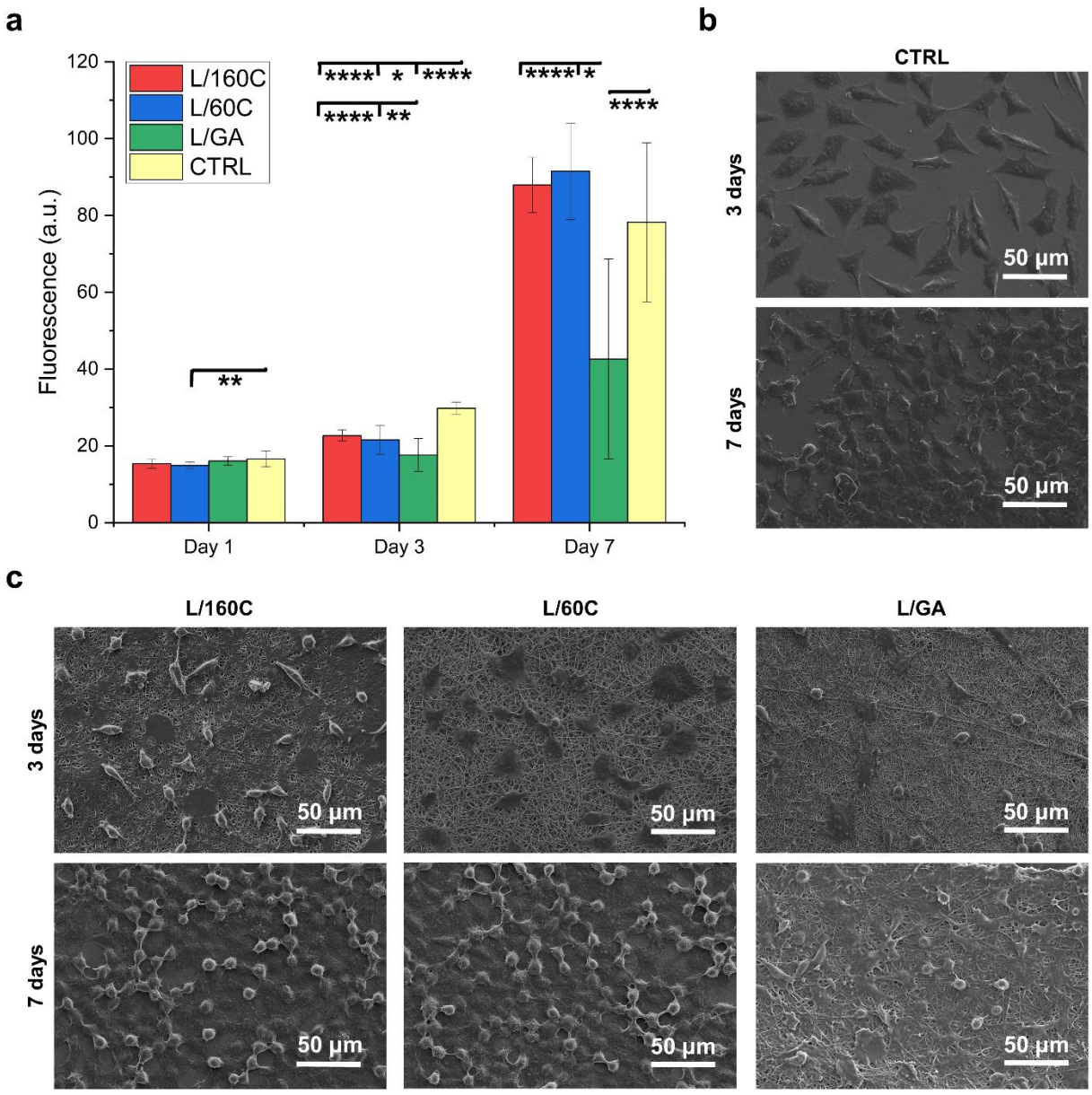

Figure 7. Viability and cell morphology of L929 fibroblast seeded on PVA-based systems containing lemon juice. a) The proliferation of L929 fibroblast cells seeded on lemon juice-enriched nanofibers and directly onto glass slides (CTRL) after 1, 3, and 7 days of culture. b) SEM images of L929 fibroblasts cultured on CTRL surface for 3 and 7 days. c) SEM images of L929 fibroblasts cultured on fibrous constructs containing lemon juice for 3 and 7 days. An increasing trend of cell viability is visible under all conditions tested, whereby on day 7 of incubation, the

cell numbers can be presented in the following order (descending): L/60C, L/160C, CTRL, and L/GA.

3.9 Biological activity

Antioxidant properties. Lemon juice is rich in vitamin C (ascorbic acid), commonly known as a strong antioxidant. In addition to vitamin C, lemon juice also contains flavonoids – other compounds with antioxidant properties.[66] Antioxidants help neutralize free radicals in the body, which can cause cell damage and contribute to the development of various diseases, including cancer and heart attack.[67] Neutralization of free radicals helps reduce the risk of inflammation. What is more, some antioxidants, such as the aforementioned vitamin C present in lemon juice, have direct anti-inflammatory properties, which means that they can inhibit inflammatory processes at various stages.[68]

To confirm the antioxidant properties of nanoplatforms prepared with the addition of lemon juice, the DPPH method was used. This test is based on measuring the ability of antioxidants to neutralize free radicals, specifically the DPPH. This radical has a characteristic purple color and absorbs visible light, with the maximum absorbance at around 517 nm. When the antioxidant reacts with DPPH, an electron transfer occurs, which causes a reduction of the free radical. As a result, the color of the solution changes from purple to yellow, and therefore, the absorbance intensity decreases (Figure 8a). The graph presenting the %inhibition of the juice samples is shown in Figure 8b. The lemon juice that was not heated shows slightly better inhibition, which for only 1% (v/v) solution reaches a value of 94.7±3.3%. For the juice after heating, this value reached 79.3±6.1%, and the color of the DPPH solution after the addition of juice and incubation changed from purple to slightly pinkish. In the case of 10% (v/v) lemon juice solutions, the inhibition was 93.6±2.6% and 89.5±1.2%, respectively. It can be seen that ascorbic acid and flavonoids are sensitive to high

temperatures. During heating, their chemical structure is degraded, which leads to a reduced ability to neutralize free radicals. Nevertheless, the results obtained are satisfactory, and since the %inhibition for a low concentration of lemon juice (1% v/v) was around 79.3%, it was confirmed that it remains a strong antioxidant, even after heat treatment.

Antibacterial properties. Lemon juice is not only a common household staple but also a natural treasure trove of antibacterial properties. The juice is rich in citric acid, which plays a pivotal role in its ability to combat bacteria.[69] This acidic environment can disrupt the cell walls of bacteria, leading to their destruction. Additionally, lemon juice contains vitamin C, which is known to boost the immune system, further aiding the fight against infections. The versatility of lemon juice extends beyond culinary uses; it has been recognized for its potential in natural cleaning products and as a food preservative due to its antibacterial effects. Its ability to inhibit the growth of bacteria makes it a valuable natural alternative to chemical-based antibacterial agents. The effect of lemon juice on the antibacterial effect against *Staphylococcus aureus* colonies was investigated through an examination of bacterial inactivation on nanofibrous samples without (W/60C) and with lemon juice (L/60C). This particular species was chosen because it is among the most prevalent microorganisms and is accountable for a broad spectrum of clinical infections.[70]

During the standard procedure, the fibrous samples were kept in the agar plates inoculated with bacteria for 24 h in the incubator. The antibacterial effect of the lemon-implemented samples was noticeable. The samples of 9 mm diameter were characterized by a zone of inhibition of 13±1 mm. The representative data is presented in Figure 8c.

Quantitative tests were also conducted to evaluate the antibacterial effect. During these tests, a bacterial solution containing 10^6 bacteria was brought into contact with the investigated fibrous hydrogels for a duration of 3 h, which is the future planned application contact time of the dressing

with the wound bed.[37] Analysis of bacterial dilutions was measured by placing these solutions on agar plates and incubating them for 24 h. The quantitative analysis shows that bacteria survival decreased to 66.7±14.1% for lemon juice-infused samples (Figure 8d).

In summary, lemon juice, with its easy accessibility and natural composition, offers a simple yet effective solution for antibacterial needs, showcasing the power of nature in maintaining health and hygiene.

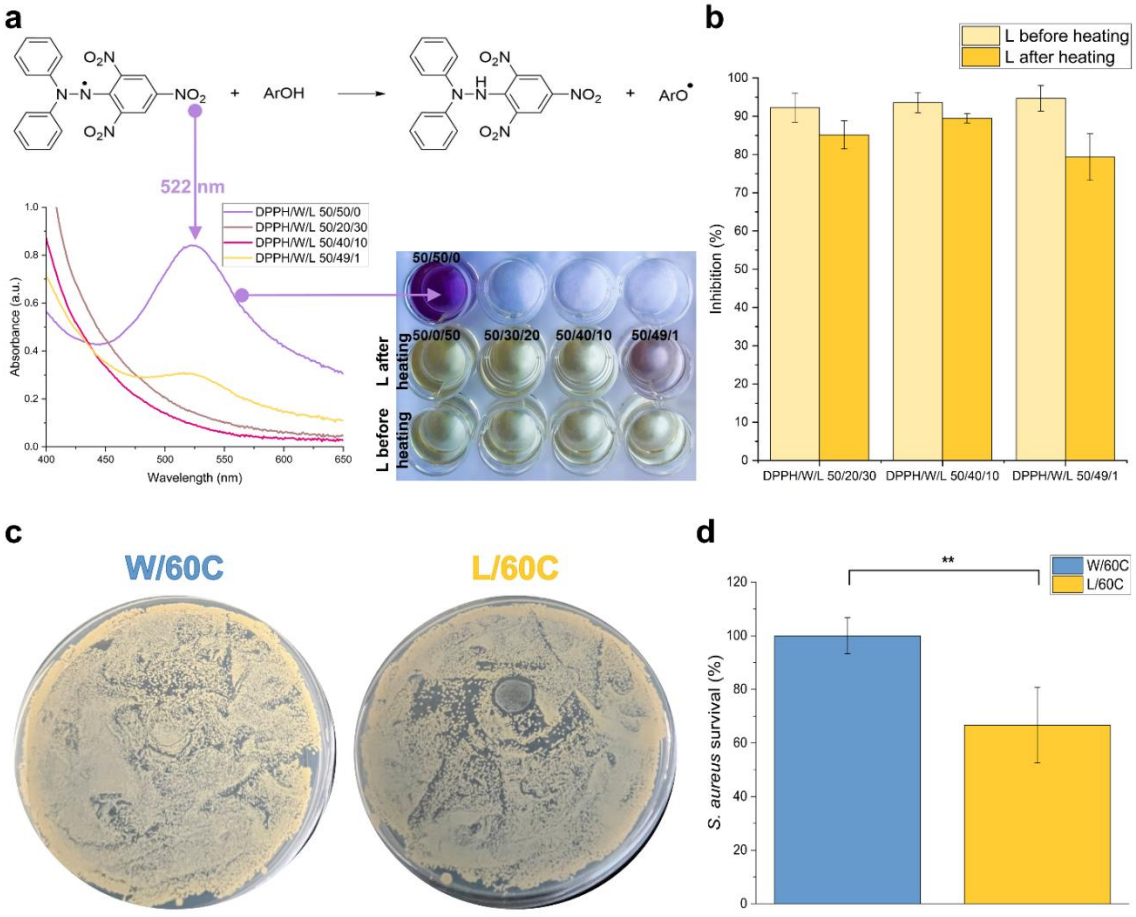

Figure 8. Antioxidant and antibacterial properties resulting from the presence of lemon juice in the developed systems. a) Reduction reaction of the stable DPPH radical with electron transfer from the antioxidant (top), absorption spectra of DPPH solution after incubation with heated lemon juice (left), and camera photo of DPPH solutions containing heated and unheated lemon juice after incubation (right). In the solutions DPPH/water/lemon juice ratio was 50/50/0, 50/20/30, 50/40/10,

and 50/49/1. b) Antioxidant properties of lemon juice, both unheated and heated, differing in concentration. Just 1% (v/v) solutions inhibit free radicals, reaching inhibition values of around 94.7% and 79.3% for unheated and heat-treated lemon juice, respectively. c) Macroscopic photos presenting zones of inhibition of *Staphylococcus aureus* colonies growing on LB agar plates on which fibrous nanofibers were placed for each tested condition: W/60C and L/60C. d) Quantitative survival of *Staphylococcus aureus* after 3 h of liquid contact with nanofibers.

4. CONCLUSIONS

This study introduces a novel low-temperature method for PVA cross-linking using freshly squeezed lemon juice. The low-temperature approach was chosen to allow further tuning of PVA-based nanoplatform properties by incorporating drugs or other biologically active molecules. The developed method takes advantage of the esterification reaction between the hydroxyl groups of PVA and the carboxyl groups of citric acid, catalyzed by the acidity of lemon juice (pH ≈ 2). These characteristics make this method a "green" cross-linking approach that is environmentally friendly, as it avoids the use of harmful substances.

PVA nanofibers were produced by electrospinning from lemon juice solutions and aqueous solutions for comparison. Low-temperature cross-linking (60 °C for 7 days) was also compared with a high-temperature approach (160 °C for 2 h) and exposure to glutaraldehyde vapors (1.0 M GA for 24 h). All systems were characterized in terms of morphology, water solubility, chemical bonds, stability over time, mechanical properties, photothermal response, and thermal stability. Their biocompatibility and – resulting from the presence of health-promoting lemon juice – the ability to inhibit free radicals and antibacterial activity were also investigated.

The results of the conducted analyses revealed that all nanoplatforms have the desired morphology, nanofibers are continuous, cylindrical, and free of beads. All systems containing lemon juice (L/NC, L/160C, L/60C, and L/GA) are insoluble in water, although L/NC looks like a porous film after 24 h of immersion. At the same time, W/NC and W/60C lost their fibrous morphology during the solubility test. This confirms the role of the lemon component as a promising cross-linker. The spectrophotometric analysis confirmed the chemical interaction between PVA and lemon juice, as well as the associated higher cross-linking efficiency compared to samples without the addition of the fruit component. These interactions are also reflected in the mechanical properties, where the higher stiffness of the cross-linked L nanofibers compared to the cross-linked W samples is observed. Moreover, samples cross-linked at low temperature, turned out to be the most deformable, which again allows to consider the developed method as optimal in terms of the material properties. The addition of lemon juice also brought further benefits related to thermal stability. This study confirmed lemon juice ability to neutralize free radicals (even in very low concentrations), which indirectly links to anti-inflammatory properties, as well as its ability to kill *S. aureus* bacteria. Therefore, the nanoplatform may be particularly beneficial to use in wound healing dressings. An additional interesting feature revealed experimentally is the photoresponsivity of the W/160C and L/160C samples, with the maximum temperature over 50 °C being reached faster by the material with the addition of lemon juice. This research has great potential and should be further expanded as it may lead to new developments in the fields of photothermal therapy, on-demand drug release, and bacteria elimination. All systems are biocompatible, with lemon additionally supporting cell growth, spread, and proliferation. The obtained results clearly indicate that the low-temperature method, apart from its effectiveness, paves the way for the developed material to be widely used in the field of biomedical engineering.

AUTHOR INFORMATION

Corresponding Author

Filippo Pierini

Department of Biosystems and Soft Matter, Institute of Fundamental Technological Research, Polish Academy of Sciences, Pawińskiego 5B, 02-106 Warsaw, Poland

e-mail address: fpierini@ippt.pan.pl

ACKNOWLEDGMENT

This work was supported by the National Science Centre (NCN) SONATA BIS Project No. 2020/38/E/ST5/00456. Figures 1, 6d, S2a, S2c, and S5a were created with BioRender. TOC was partially created with BioRender and images from Flaticon.com. S.S.Z. acknowledges the financial support from HORIZON TMA MSCA Postdoctoral Fellowships – European Fellowships (HORIZON-TMA-MSCA-PF-EF) action program under the call MSCA Postdoctoral Fellowships 2021 (HORIZON-MSCA-2021-PF-01), grant agreement No. 101068036, "SuSCoFilter". F.P. acknowledges the financial support from the Polish Ministry of Science and Higher Education.

REFERENCES

(1) Maitra, J.; Shukla, V. K. Cross-Linking in Hydrogels - A Review. *J. Polym. Sci.* **2014**, *4* (2), 25–31. DOI: 10.5923/j.ajps.20140402.01.

(2) *Polymer Grafting and Crosslinking*; Bhattacharya, A., Rawlins, J. W., Ray, P., Eds.; John Wiley & Sons, Inc.: Hoboken, NJ, USA, 2008. DOI: 10.1002/9780470414811.

(3) Mehta, P.; Sharma, M.; Devi, M. Hydrogels: An Overview of Its Classifications, Properties, and Applications. *J. Mech. Behav. Biomed. Mater.* **2023**, *147* (1), 106145. DOI: 10.1016/j.jmbbm.2023.106145.

(4) Ahmed, E. M. Hydrogel: Preparation, Characterization, and Applications: A Review. *J. Advanc. Res.* **2015**, *6* (2), 105–121. DOI: 10.1016/j.jare.2013.07.006.

(5) Liang, Y.; He, J.; Guo, B. Functional Hydrogels as Wound Dressing to Enhance Wound Healing. *ACS Nano* **2021**, *15* (8), 12687–12722. DOI: 10.1021/acsnano.1c04206.

(6) Norahan, M. H.; Pedroza-González, S. C.; Sánchez-Salazar, M. G.; Álvarez, M. M.; Trujillo de Santiago, G. Structural and Biological Engineering of 3D Hydrogels for Wound Healing. *Bioact. Mater.* **2023**, *24*, 197–235. DOI: 10.1016/j.bioactmat.2022.11.019.

(7) Bernhard, S.; Tibbitt, M. W. Supramolecular Engineering of Hydrogels for Drug Delivery. *Adv. Drug Deliv. Rev.* **2021**, *171* (5), 240–256. DOI: 10.1016/j.addr.2021.02.002.

(8) Kesharwani, P.; Bisht, A.; Alexander, A.; Dave, V.; Sharma, S. Biomedical Applications of Hydrogels in Drug Delivery System: An Update. *J. Drug Deliv. Sci. Technol.* **2021**, *66* (2), 102914. DOI: 10.1016/j.jddst.2021.102914.

(9) Drury, J. L.; Mooney, D. J. Hydrogels for Tissue Engineering: Scaffold Design Variables and Applications. *Biomaterials* **2003**, *24* (24), 4337–4351. DOI: 10.1016/s0142-9612(03)00340-5.

(10) Luo, R.; Xiang, X.; Jiao, Q.; Hua, H.; Chen, Y. Photoresponsive Hydrogels for Tissue Engineering. *ACS Biomater. Sci. Eng.* **2024**, *10* (6), 3612–3630. DOI: 10.1021/acsbiomaterials.4c00314.

(11) Lee, J.-H.; Kim, H.-W. Emerging Properties of Hydrogels in Tissue Engineering. *J. Tissue Eng.* **2018**, *9* (6337), 2041731418768285. DOI: 10.1177/2041731418768285.

(12) Cirulli, A.; Neves Borgheti-Cardoso, L.; Torras, N.; García-Díaz, M.; Martínez, E. Hydrogels as Tissue Barriers. In *Hydrogels for tissue engineering and regenerative medicine*; Elsevier, 2024; pp 433–466. DOI: 10.1016/B978-0-12-823948-3.00017-8.

(13) Li, Y.; Wang, X.; Fu, Y.-N.; Wei, Y.; Zhao, L.; Tao, L. Self-Adapting Hydrogel to Improve the Therapeutic Effect in Wound-Healing. *ACS Appl. Mater. Interfaces* **2018**, *10* (31), 26046–26055. DOI: 10.1021/acsami.8b08874.

(14) Teodorescu, M.; Bercea, M.; Morariu, S. Biomaterials of PVA and PVP in Medical and Pharmaceutical Applications: Perspectives and Challenges. *Biotechnol. Adv.* **2019**, *37* (1), 109–131. DOI: 10.1016/j.biotechadv.2018.11.008.

(15) Suleiman, G. S. A.; Zeng, X.; Chakma, R.; Wakai, I. Y.; Feng, Y. Recent Advances and Challenges in Thermal Stability OfPVA -based Film: A Review. *Polym. Adv. Technol.* **2024**, *35* (2), e6327. DOI: 10.1002/pat.6327.

(16) Alipoori, S.; Mazinani, S.; Aboutalebi, S. H.; Sharif, F. Review of PVA-Based Gel Polymer Electrolytes in Flexible Solid-State Supercapacitors: Opportunities and Challenges. *J. Energy Storage* **2020**, *27* (1), 101072. DOI: 10.1016/j.est.2019.101072.

(17) Yang, X.; Wang, S.; Zhang, X.; Ye, C.; Wang, S.; An, X. Development of PVA-Based Microsphere as a Potential Embolization Agent. *Mater. Sci. Eng. C Mater. Biol. Appl.* **2022**, *135* (2), 112677. DOI: 10.1016/j.msec.2022.112677.

(18) Park, J.-C.; Ito, T.; Kim, K.-O.; Kim, K.-W.; Kim, B.-S.; Khil, M.-S.; Kim, H.-Y.; Kim, I.-S. Electrospun Poly(Vinyl Alcohol) Nanofibers: Effects of Degree of Hydrolysis and Enhanced Water Stability. *Polym. J.* **2010**, *42* (3), 273–276. DOI: 10.1038/pj.2009.340.

(19) Chen, Y.; Hao, Y.; Mensah, A.; Lv, P.; Wei, Q. Bio-Inspired Hydrogels with Fibrous Structure: A Review on Design and Biomedical Applications. *Biomater. Adv.* **2022**, *136* (19), 212799. DOI: 10.1016/j.bioadv.2022.212799.

(20) Li, Y.; Zhu, J.; Cheng, H.; Li, G.; Cho, H.; Jiang, M.; Gao, Q.; Zhang, X. Developments of Advanced Electrospinning Techniques: A Critical Review. *Adv. Mater. Technol.* **2021**, *6* (11), 2100410. DOI: 10.1002/admt.202100410.

(21) Yarin, A. L.; Koombhongse, S.; Reneker, D. H. Bending Instability in Electrospinning of Nanofibers. *J. Appl. Phys.* **2001**, *89* (5), 3018–3026. DOI: 10.1063/1.1333035.

(22) Zakrzewska, A.; Zargarian, S. S.; Rinoldi, C.; Gradys, A.; Jarząbek, D.; Zanoni, M.; Gualandi, C.; Lanzi, M.; Pierini, F. Electrospun Poly(Vinyl Alcohol)-Based Conductive Semi-Interpenetrating Polymer Network Fibrous Hydrogel: A Toolbox for Optimal Cross-Linking. *ACS Mater. Au* **2023**, *3* (5), 464–482. DOI: 10.1021/acsmaterialsau.3c00025.

(23) Liao, H.; Liu, Y.; Wang, Q.; Duan, W. Structure and Properties of Porous Poly(Vinyl Alcohol) Hydrogel Beads Prepared through a Physical-Chemical Crosslinking Method. *J. Appl. Polym. Sci.* **2018**, *135* (26), 46402. DOI: 10.1002/app.46402.

(24) Arora, B.; Tandon, R.; Attri, P.; Bhatia, R. Chemical Crosslinking: Role in Protein and Peptide Science. *Curr. Protein Pept. Sci.* **2017**, *18* (9), 946–955. DOI: 10.2174/1389203717666160724202806.

(25) Teixeira, M. A.; Antunes, J. C.; Amorim, M. T. P.; Felgueiras, H. P. Optimization of the Crosslinking Process with Glutaraldehyde Vapor in PVA Based Electrospun Membranes to Wound Dressings Applications. In *Proceedings of 2nd International Online-Conference on Nanomaterials*; MDPI: Basel, Switzerland, 2020; Vol. 4, p 7906. DOI: 10.3390/IOCN2020-07906.

(26) Baykara, D.; Pilavci, E.; Cesur, S.; Ilhan, E.; Ulag, S.; Sengor, M.; Kijeńska-Gawrońska, E.; Gunduz, O. Controlled Release of Gentamicin from Electrospun Poly(Vinyl Alcohol)/Gelatin Nanofibers: The Effect of Crosslinking Time Using Glutaraldehyde Vapor. *ChemistrySelect* **2023**, *8* (5), e202203681. DOI: 10.1002/slct.202203681.

(27) Coşkuner Filiz, B.; Basaran Elalmis, Y.; Bektaş, İ. S.; Kantürk Figen, A. Fabrication of Stable Electrospun Blended Chitosan-Poly(Vinyl Alcohol) Nanofibers for Designing Naked-Eye Colorimetric Glucose Biosensor Based on GOx/HRP. *Int. J. Biol. Macromol.* **2021**, *192*, 999–1012. DOI: 10.1016/j.ijbiomac.2021.10.048.

(28) Ullah, S.; Hashmi, M.; Hussain, N.; Ullah, A.; Sarwar, M. N.; Saito, Y.; Kim, S. H.; Kim, I. S. Stabilized Nanofibers of Polyvinyl Alcohol (PVA) Crosslinked by Unique Method for Efficient Removal of Heavy Metal Ions. *J. Water Proc. Engineering* **2020**, *33*, 101111. DOI: 10.1016/j.jwpe.2019.101111.

(29) Hong, X.; He, J.; Zou, L.; Wang, Y.; Li, Y. V. Preparation and Characterization of High Strength and High Modulus PVA Fiber via Dry-Wet Spinning with Cross-Linking of Boric Acid. *J. Appl. Polym. Sci.* **2021**, *138* (47), 51394.

(30) Lei, L. I.; Guang-lun, L. E. I.; Chuan-jin, Y. A. O.; Xue-mei, G. A. O.; Jia-yu, Y. O. U. Study on Elasticity and Swelling Behavior of PVA Hydrogel. *Polym. Bull.* **2013**, *26* (6), 39–43.

(31) Nataraj, D.; Reddy, R.; Reddy, N. Crosslinking Electrospun Poly (Vinyl) Alcohol Fibers with Citric Acid to Impart Aqueous Stability for Medical Applications. *Eur. Polym. J.* **2020**, *124* (1), 109484. DOI: 10.1016/j.eurpolymj.2020.109484.

(32) Ghorpade, V. S.; Dias, R. J.; Mali, K. K.; Mulla, S. I. Citric Acid Crosslinked Carboxymethylcellulose-Polyvinyl Alcohol Hydrogel Films for Extended Release of Water Soluble Basic Drugs. *J. Drug Deliv. Sci. Technol.* **2019**, *52* (5), 421–430. DOI: 10.1016/j.jddst.2019.05.013.

(33) Liguori, A.; Zhao, J.; Di Gesù, R.; De Marco, R.; Gualandi, C.; Calonghi, N.; Pollicino, A.; Gentilucci, L.; Focarete, M. L. Peptide Direct Growth on Poly(Acrylic Acid)/Poly(Vinyl Alcohol) Electrospun Fibers Coated with Branched Poly(Ethylenimine):

A Solid-Phase Approach for Scaffolds Biofunctionalization. *Colloids Surf. B Biointerfaces* **2024**, *241*, 114052. DOI: 10.1016/j.colsurfb.2024.114052.

(34) Yang, J.; Chen, Y.; Zhao, L.; Zhang, J.; Luo, H. Constructions and Properties of Physically Cross-Linked Hydrogels Based on Natural Polymers. *Polym. Rev.* **2022**, *63* (3), 574–612. DOI: 10.1080/15583724.2022.2137525.

(35) Adelnia, H.; Ensandoost, R.; Shebbrin Moonshi, S.; Gavgani, J. N.; Vasafi, E. I.; Ta, H. T. Freeze/Thawed Polyvinyl Alcohol Hydrogels: Present, Past and Future. *Eur. Polym. J.* **2022**, *164* (11), 110974. DOI: 10.1016/j.eurpolymj.2021.110974.

(36) Nain, A.; Dahiya, S.; Chahal, R. P.; Dhanda, E. Ultraviolet (UV) Irradiated Induced Changes in Optical Properties of PVA/Ag Nanocomposite Films. *Phys. Scr.* **2022**, *97* (4), 045817. DOI 10.1088/1402-4896/ac5ce2.

(37) Kosik-Kozioł, A.; Nakielski, P.; Rybak, D.; Frączek, W.; Rinoldi, C.; Lanzi, M.; Grodzik, M.; Pierini, F. Adhesive Antibacterial Moisturizing Nanostructured Skin Patch for Sustainable Development of Atopic Dermatitis Treatment in Humans. *ACS Appl. Mater. Interfaces* **2024**, *16* (25), 32128–32146. DOI: 10.1021/acsami.4c06662.

(38) Miraftab, M.; Saifullah, A. N.; Çay, A. Physical Stabilisation of Electrospun Poly(Vinyl Alcohol) Nanofibres: Comparative Study on Methanol and Heat-Based Crosslinking. *J. Mater. Sci.* **2015**, *50* (4), 1943–1957. DOI: 10.1007/s10853-014-8759-1.

(39) Ali, N. M.; Kareem, A. A.; Polu, A. R. Effect of Glycerin on Electrical and Thermal Properties of PVA/Copper Sulphate Gel Polymer Electrolytes. *J. Inorg. Organomet. Polym. Mater.* **2022**, *32* (10), 4070–4076. DOI: 10.1007/s10904-022-02417-7.

(40) Wunderlich, B. *Thermal Analysis of Polymeric Materials*; Springer: Berlin/Heidelberg, 2005; p 781. DOI: 10.1007/b137476.

(41) Schiffman, J. D.; Schauer, C. L. Cross-Linking Chitosan Nanofibers. *Biomacromolecules* **2007**, *8* (2), 594–601. DOI: 10.1021/bm060804s.

(42) Nakielski, P.; Rybak, D.; Jezierska-Woźniak, K.; Rinoldi, C.; Sinderewicz, E.; Staszkiewicz-Chodor, J.; Haghighat Bayan, M. A.; Czelejewska, W.; Urbanek, O.; Kosik-Kozioł, A.; Barczewska, M.; Skomorowski, M.; Holak, P.; Lipiński, S.; Maksymowicz, W.; Pierini, F. Minimally Invasive Intradiscal Delivery of BM-MSCs via Fibrous Microscaffold Carriers. *ACS Appl. Mater. Interfaces* **2023**, *15* (50), 58103–58118. DOI: 10.1021/acsami.3c11710.

(43) Baliyan, S.; Mukherjee, R.; Priyadarshini, A.; Vibhuti, A.; Gupta, A.; Pandey, R. P.; Chang, C.-M. Determination of Antioxidants by DPPH Radical Scavenging Activity and Quantitative Phytochemical Analysis of Ficus Religiosa. *Molecules* **2022**, *27* (4), 1326. DOI: 10.3390/molecules27041326.

(44) Santos, C.; Silva, C. J.; Büttel, Z.; Guimarães, R.; Pereira, S. B.; Tamagnini, P.; Zille, A. Preparation and Characterization of Polysaccharides/PVA Blend Nanofibrous Membranes by Electrospinning Method. *Carbohydr. Polym.* **2014**, *99*, 584–592. DOI: 10.1016/j.carbpol.2013.09.008.

(45) Fahami, A.; Fathi, M. Fabrication and Characterization of Novel Nanofibers from Cress Seed Mucilage for Food Applications. *J. Appl. Polym. Sci.* **2018**, *135* (6), 45811. DOI: 10.1002/app.45811.

(46) Mansur, H. S.; Sadahira, C. M.; Souza, A. N.; Mansur, A. A. P. FTIR Spectroscopy Characterization of Poly (Vinyl Alcohol) Hydrogel with Different Hydrolysis Degree and Chemically Crosslinked with Glutaraldehyde. *Mater. Sci. Eng. C* **2008**, *28* (4), 539–548. DOI: 10.1016/j.msec.2007.10.088.

(47) Pimpang, P.; Rattiphorn, S.; Supab, C. Effect of Concentration of Citric Acid on Size and Optical Properties of Fluorescence Graphene Quantum Dots Prepared by Tuning Carbonization Degree. *Chiang Mai J. Sci.* **2018**, *45* (5), 2005–2014. DOI: –

(48) Ma, X.; Zhong, W.; Zhao, J.; Suib, S. L.; Lei, Y. "Self-Heating" Enabled One-Pot Synthesis of Fluorescent Carbon Dots. *Eng. Sci.* **2020**, *9*, 44–49. DOI: 10.30919/es8d805.

(49) Sau, S.; Pandit, S.; Kundu, S. Crosslinked Poly (Vinyl Alcohol): Structural, Optical and Mechanical Properties. *Surf. Interfaces* **2021**, *25*, 101198. DOI: 10.1016/j.surfin.2021.101198.

(50) Guan, H.; Zhang, W. Delocalization of Π-Electron in Graphitic Carbon Nitride to Promote Its Photocatalytic Activity for Hydrogen Evolution. *ChemCatChem* **2019**, *11* (22), 5633–5641. DOI: 10.1002/cctc.201901314.

(51) Taranekar, P.; Fulghum, T.; Patton, D.; Ponnapati, R.; Clyde, G.; Advincula, R. Investigating Carbazole Jacketed Precursor Dendrimers: Sonochemical Synthesis, Characterization, and Electrochemical Crosslinking Properties. *J. Am. Chem. Soc.* **2007**, *129* (41), 12537–12548. DOI: 10.1021/ja074007t.

(52) Tomas, A.; Aslan, L.; Muñoz, A.; Ródenas, M.; Vera, T.; Borrás, E.; Coddeville, P.; Fittschen, C. Photolysis of Multifunctional Carbonyl Compounds under Natural Irradiation at EUPHORE. *Atmos. Environ.* **2021**, *253*, 118352. DOI: 10.1016/j.atmosenv.2021.118352.

(53) Picollo, M.; Aceto, M.; Vitorino, T. UV-Vis Spectroscopy. *Phys. Sci. Rev.* **2019**, *4* (4). DOI: 10.1515/psr-2018-0008.

(54) Anouar, E. H.; Gierschner, J.; Duroux, J.-L.; Trouillas, P. UV/Visible Spectra of Natural Polyphenols: A Time-Dependent Density Functional Theory Study. *Food Chem.* **2012**, *131* (1), 79–89. DOI: 10.1016/j.foodchem.2011.08.034.

(55) Lyu, W.; Yuan, B.; Liu, S.; Simon, J. E.; Wu, Q. Assessment of Lemon Juice Adulteration by Targeted Screening Using LC-UV-MS and Untargeted Screening Using UHPLC-QTOF/MS with Machine Learning. *Food Chem.* **2022**, *373* (2), 131424. DOI: 10.1016/j.foodchem.2021.131424.

(56) Maria, T. M. C.; de Carvalho, R. A.; Sobral, P. J. A.; Habitante, A. M. B. Q.; Solorza-Feria, J. The Effect of the Degree of Hydrolysis of the PVA and the Plasticizer Concentration on the Color, Opacity, and Thermal and Mechanical Properties of Films Based on PVA and Gelatin Blends. *J. Food Eng.* **2008**, *87* (2), 191–199. DOI: 10.1016/j.jfoodeng.2007.11.026.

(57) Hong, X.; Zou, L.; Zhao, J.; Li, C.; Cong, L. Dry-Wet Spinning of PVA Fiber with High Strength and High Young's Modulus. *IOP Conf. Ser.: Mater. Sci. Eng.* **2018**, *439* (4), 042011. DOI: 10.1088/1757-899X/439/4/042011.

(58) Pereao, O.; Bode-Aluko, C.; Laatikainen, K.; Nechaev, A.; Petrik, L. Morphology, Modification and Characterisation of Electrospun Polymer Nanofiber Adsorbent Material Used in Metal Ion Removal. *J. Polym. Environ.* **2019**, *27* (9), 1843–1860. DOI: 10.1007/s10924-019-01497-w.

(59) Ortega-Toro, R. Development and Characterization of Corn Starch Films by Blending with More Hydrophobic Compounds. Doctoral dissertation, 2015.

(60) Shi, R.; Zhang, Z.; Liu, Q.; Han, Y.; Zhang, L.; Chen, D.; Tian, W. Characterization of Citric Acid/Glycerol Co-Plasticized Thermoplastic Starch Prepared by Melt Blending. *Carbohydr. Polym.* **2007**, *69* (4), 748–755. DOI: 10.1016/j.carbpol.2007.02.010.

(61) Zhou, Y.; Chu, R.; Fan, L.; Meng, X.; Zhao, J.; Wu, G.; Li, X.; Jiang, X.; Sun, F. Study on the Mechanism and Performance of Polymer Gels ByTE AndPVA Chemical Cross-linking. *J. Appl. Polym. Sci.* **2022**, *139* (17). DOI: 10.1002/app.52043.

(62) Nielsen, L. E. Cross-Linking–Effect on Physical Properties of Polymers. *J. Macromol. Sci. Chem. A* **1969**, *3* (1), 69–103. DOI: 10.1080/15583726908545897.

(63) Bermejo, J. S.; Ugarte, C. M. Influence of Cross-linking Density on the Glass Transition and Structure of Chemically Cross-linked PVA: A Molecular Dynamics Study. Macromol. *Theory Simul.* **2009**, *18* (6), 317–327. DOI: 10.1002/mats.200900032.

(64) Koosha, M.; Mirzadeh, H. Electrospinning, Mechanical Properties, and Cell Behavior Study of Chitosan/PVA Nanofibers. *J. Biomed. Mater. Res. A* **2015**, *103* (9), 3081–3093. DOI: 10.1002/jbm.a.35443.

(65) Holland, B. J.; Hay, J. N. The Thermal Degradation of Poly(Vinyl Alcohol). *Polymer* **2001**, *42* (16), 6775–6783. DOI: 10.1016/S0032-3861(01)00166-5.

(66) Rietjens, I. M. C. M.; Boersma, M. G.; Haan, L. de; Spenkelink, B.; Awad, H. M.; Cnubben, N. H. P.; van Zanden, J. J.; Woude, H. van der; Alink, G. M.; Koeman, J. H. The Pro-Oxidant Chemistry of the Natural Antioxidants Vitamin C, Vitamin E, Carotenoids and Flavonoids. *Environ. Toxicol. Pharmacol* **2002**, *11* (3–4), 321–333. DOI: 10.1016/s1382-6689(02)00003-0.

(67) Sharma, N. Free Radicals, Antioxidants and Disease. *Biol. Med. (Aligarh)* **2014**, *6* (3), 1000214. DOI: 10.4172/0974-8369.1000214.

(68) Wong, S. K.; Chin, K.-Y.; Ima-Nirwana, S. Vitamin C: A Review on Its Role in the Management of Metabolic Syndrome. *Int. J. Med. Sci.* **2020**, *17* (11), 1625–1638. DOI: 10.7150/ijms.47103.

(69) Nagoba, B.; R, R.; Wadher, B.; Gandhi, R.; AK, R.; Selkar, S.; Hartalkar, A. Citric Acid Treatment of Surgical Site Infections: A Prospective Open Study. *Wound Practice and Research* **2011**, *19* (2), 82–86. DOI: 10.13140/rg.2.1.1266.1524.

(70) Tong, S. Y. C.; Davis, J. S.; Eichenberger, E.; Holland, T. L.; Fowler, V. G. *Staphylococcus Aureus* Infections: Epidemiology, Pathophysiology, Clinical Manifestations, and Management. *Clin. Microbiol. Rev.* **2015**, *28* (3), 603–661. DOI: 10.1128/CMR.00134-14.

TABLE OF CONTENT